# 國立交通大學

## 機械工程學系

## 碩士論文

# 生醫應用上之蠕動式微幫浦性能探討

# Analysis of the Performance on Peristaltic Micropumps for Biomedical Applications

研究生：關 恕

指導教授：陳俊勳　教授

中 華 民 國 九 十 五 年 六 月

# 生醫應用上之蠕動式微幫浦性能探討

# Analysis of the Performance on Peristaltic Micropumps for Biomedical Applications


研究生　：關　恕　　Student：Kuan Shu

指導教授：陳俊勳　　Advisor：Chiun-Hsun Chen

國 立 交 通 大 學

機 械 工 程 學 系

碩 士 論 文


A Thesis

Submitted to Department of Mechanical Engineering

College of Engineering

National Chiao Tung University

In Partial Fulfiillment of the Requirements

For the Degree of

Master of Science

In Mechanical Engineering

June 2006

Hsinchu, Taiwan, Republic of China

中 華 民 國 九 十 五 年 六 月

# 國立交通大學

## 論文口試委員會審定書

本校 機械工程 學系碩士班 關恕 君

所提論文(中文) 生醫應用上之蠕動式微幫浦性能探討

(英文) Analysis of the Performance on Peristaltic Micropumps for Biomedical Application

合於碩士資格水準、業經本委員會評審認可。

口試委員：張淩晨 陳菊蘭

陳俊勳

指導教授：陳俊勳

系主任：傅武雄 教授

中華民國 95 年 6 月 8 日

生醫應用上之蠕動式微幫浦性能探討

學生：關 恕　　指導教授：陳俊勳

國立交通大學機械工程學系碩士班

## 摘要

本論文描述利用微機電系統技術的壓電無閥門蠕動式微型幫浦的設計、製程與應用。微幫浦驅動原理在於 PZT 受到驅動訊號使得致動薄膜做往覆週期的運動。如此的裝置就如同活塞提供動力驅動微升等級的流體，如此可利用到許多生醫應用上的實驗室晶片。因此，本論文便是針對微幫浦的性能分析而探討，主要可分成兩部分。

首先，我們關注的是系統與週遭環境對輸出共振頻率的影響。為提高蠕動式微型幫浦的輸出能力，從理論上分析了負載流體對致動薄膜動態特性的影響規律。除了流體的密度以及黏滯性會對附加質量及附加阻尼造成影響外，流室深度以及驅動相位亦會影響致動薄膜動態特性，造成頻率位移現象。其次，流體的傳輸能力與電路的設計是具有緊密的連結。因此藉由適當電路設計的改良能有效提升傳輸流量 1.9~2.8 倍。

# Analysis of the Performance on Peristaltic Micropumps for Biomedical Applications

Student：Kuan Shu Advisor：Chiun-Hsun Chen

Department of Mechanical Engineering

National Chiao Tung University

## Abstract

A valveless peristaltic micropump based on piezoelectric actuation was designed and fabricated. The pump diaphragms are excited by applying pulse signal voltages to three lead zirconate titanate (PZT) disks on glass diaphragm. Such diaphragm structure acts as a “piston” to provide power for the handling of microliter-scaled fluid volumes desired in many lab-on-a-chip chemical and biomedical applications. A high-performance micropump was investigated for this purpose. The paper contains mainly two parts as follows.

First, we are concerned with the interactions between a system and its environment for the influence on output resonance frequency. Analytical results for frequency shift was presented to show that not only does the added mass and added damping depend on both the fluid density and viscosity, the chamber height and actuated signal are as well. Second, the driving circuit can be closely linked with the fluid transport related to the pump performance. Therefore, the improvement design for driving circuit can enhance pump flow rate performance up to 1.9~2.8 times.

# Contents

Abstract (in Chinese) ..... ……...3

Abstract ……...4

List of figure .....7

List of table .....11

Acknowledgement (in Chinese) .....12

Chapter 1.....13

Inefinitesimal Machinery: An Intrigued Word.....13

1.1 Introduction……..13

1.2 Literature review…….....16

Chapter 2 ……26

The Damping Effects on the Micro-diaphragm.....…26

2.1 Piezoelectric materials……..26

2.2 Performance of the frequency-dependent flow rate……. 28

2.2.1 A simple spring-mass-damper system under simple harmonic excitation ..... ….30

2.2.2 Complex representations ..... 34

2.3 Analysis of the simplified micropump for the flow rate…….. 35

2.4 The added mass and added damping……40

2.5 Analysis of the frequency shift with the interactions exerted on the micro-diaphragm……...43

2.6 The system dynamic for a peristaltic micropump…… 48

2.6.1 Electrical field ..... 49
2.6.2 Mechanical field ..... 53
2.6.3 Governing equations..... 55
2.6.4 Flow field..... 65

Chapter 3…..…68

Fabrication and Test.....…68

3.1 Design and fabrication of a peristaltic micropump…….. 68

3.2 Experimental setup……... 72

3.3 Experiments and results……73

Chapter 4….....90

Results and Discussion .....90

4.1 Discussion and conclusion……... 90

4.2 Outlook……91

References.....93

# List of Figure


Fig. 1 A Typical Biochip Layout—Component ..... 15

Fig. 2 Valveless rectification micropumps ..... 19

Fig. 3 Tesla pump: (a) design example (b) rectification effect..... 19

Fig. 4 Flow rate range of different pump principles. ..... 20

Fig. 5 Actuation sequences of a peristaltic micropump based on piezoelectric actuation micropump..... 24

Fig. 6 The flow chart of a six-phase driving peristaltic micropump..... 25

Fig. 7 The deformation of a piezoelectric device when subject to an electrical voltage..... 27

Fig. 8 A simplified diaphragm micropump viscously damped system with harmonic excitation. ..... 31

Fig. 9 The schematic of a diaphragm micropump for analysis of flow rate 36

Fig. 10 Vibration of a beam of uniform cross section loaded at the middle with a block of weight W ..... 41

Fig. 11 A simplified model for diaphragm micropump ..... 45

Fig. 12 The illustration of frequency shift ..... 48

Fig. 13 The general environment for the system ..... 49

Fig. 14 Definition of the 3, 4 and6 phase durations..... 50

Fig. 15 Actuation sequences of a 2-phase peristaltic micropump ..... 51

Fig. 16 Definition of the 2-phase durations. ..... 51

Fig. 17 A top view of the stresses obtained from FEM analysis in the 1st mode frequency..... 54

Fig. 18 The stress distributed at different position in the 1st mode..... 55

Fig. 19 **a.** Schematic of the cross section of a piezo-Pyrex-diaphragm

bi-layer **b.** Deflection of the pump diaphragm $D_1$: diameter of PZT; $D_2$: diameter of Pyrex; $S$: distance between Pyrex and PZT edges; diaphragm thickness $t_1$ =191μm and $t_2$ = 150 μm ..... 58
Fig. 20 The solution algorithm for piezo-diaphragm-fluid coupled solver . 60
Fig. 21 The three layers model under 100Hz sinusoidal excitation (water, 100V). Grids at the center area of each layer are denser. ..... 61
Fig. 22 Transient behavior of a point centered on diaphragm-fluid interface ..... 62
Fig. 23 The photo of the finished diffuser/nozzle ..... 62
Fig. 24 The modal shape analysis for PZT and Si diaphragm bi-layer ..... 65
Fig. 25 (a) Schematic of the peristaltic micropump (b) SEM photo of the step channel (c) Recirculation region ..... 66
Fig. 26 Schematic representation of the rectangular channel ..... 66
Fig. 27 Schematic of peristaltic micropumps..... 69
Fig. 28 Glass etching process..... 70
Fig. 29 Silicon etching process. ..... 71
Fig. 30 The photomask of channel and chamber ..... 71
Fig. 31 The complete peristaltic micropump ..... 71
Fig. 32 The schematic of the experimental setup..... 73
Fig. 33 Displacement of the middle moving diaphragm as a function of phase frequency at 100 $V_{pp}$(4P16) ..... 74
Fig. 34 Flow rate *vs.* phase frequency at 100 $V_{pp}$ ..... 75
Fig. 35 Displacement of the middle moving diaphragm as a function of phase frequency at 100 $V_{pp}$ （4P20）..... 76
Fig. 36 Flow rate *vs.* phase frequency at 100 $V_{pp}$ (4P20)..... 77
Fig. 37 The displacement frequency of 2-phase sequence ..... 78

Fig. 38 The displacement of diaphragm versus the driving frequency at 100 V(4P10)..... 78
Fig. 39 The Flow rate of pumping versus the driving frequency at 100 V (4P10)..... 79
Fig. 40 The displacement of diaphragm versus the driving frequency for different working fluids. ..... 79
Fig. 41 The 3-phase sequence displacement frequency response versus the chamber height..... 80
Fig. 42 The 4-phase sequence displacement frequency response versus the chamber height..... 81
Fig. 43 The 6-phase sequence displacement frequency response versus the chamber height..... 82
Fig. 44 4-phase three chambers driving..... 82
Fig. 45 4-phase the only middle chamber driving ..... 83
Fig. 46 The charging and discharging loop of the differential amplifier..... 84
Fig. 47 The displacement vs. frequency in 3-phase sequence by reducing the collector resistance from 50 K to 10 K Ohm..... 85
Fig. 48 The flow rate vs. frequency in 3-phase sequence by reducing the collector resistance from 50 K to 10 K Ohm..... 85
Fig. 49 The displacement vs. frequency in 4-phase sequence by reducing the collector resistance from 50 K to 10 K Ohm..... 86
Fig. 50 The flow rate vs. frequency in 4-phase sequence by reducing the collector resistance from 50 K to 10 K Ohm..... 86
Fig. 51 The displacement vs. frequency in 6-phase sequence by reducing the collector resistance from 50 K to 10 K Ohm..... 87
Fig. 52 The flow rate vs. frequency in 6-phase sequence by reducing the collector resistance from 50 K to 10 K Ohm..... 87

Fig. 53 The displacement vs. frequency operated in +80 V to -20 V, +50 V to -50 V and +20 V to -80 V deferential outputs ..... 88
Fig. 54 The flow rate vs. frequency operated in +80 V to -20 V, +50 V to -50 V and +20 V to -80 V deferential outputs..... 89

# List of Table

Table 1 Mechanical pumping principles ..... 17

Table 2 The comparison between cycle frequency and driving sequence..... 51

Table 3 The cycle frequency factor..... 53

Table 4 Properties of PZT-5H ..... 56

Table 5 Fluid properties ..... 59

# Acknowledgement (in Chinese)

在交大兩年的碩士班生活中，首先要感謝陳俊勳老師，讓我順利的完成研究所學業，在學術上提供一個跨領域的學習機會，讓我們可以接觸不同領域的知識。在此亦感謝國立成功大學的張凌昇老師以及南台科技大學的許藝菊老師在百忙之中給予本論文的批評與指正，使本論文更趨完善，在此致上最高的敬意。

在研究的生活過程中，深受生命晶片實驗室成員的幫忙與指教，首先感謝松儒以及垣杰在實驗及電路上提供不少建議與協助，以及在模擬上相互成長的國華、耀文、偉雄與念暉。其次感謝宜良、明燦、瑭原、智淵、鎵豪、南江、敏峰、浩凱、浩君與交大的同學嘉鴻、靜慈。還有其它無法一一列入的研究夥伴，謝謝你們長期的陪伴與照顧，有你們的陪伴，使得兩年的研究生活，增添許多樂趣與回憶。

更感謝的是我的父母，他們給我最大的支持，在我失落時給我精神的鼓勵，讓我順利完成學業，無後顧之憂。僅以本研究獻給所有關愛我的人。

# CHAPTER 1
# INFINITESIMAL MACHINERY: AN INTRIGUED WORD

## 1.1 Introduction

Is there plenty of room at the bottom? A brilliant idea was presented by Richard P. Feynman on December 26, 1959, at the annual meeting of the America Physical Society at the California Institute of Technology [1]. The problem seems like a good idea in theory, but in practice it has recently proved that there is a strong trend for miniaturization using integrated circuit (IC) fabrication process, such as etching, photolithography, deposition, bonding and so on. This trend results on one hand from the fact that small components and system perform differently. Micro-electro -mechanical system (MEMS) has been opened new thrusts into the world and make it possible to fabricate small size devices and systems with high functionality, precision, and performance. Based on these characteristics, MEMS devices and systems have found some applications, such as automobile, aerospace, communication, medical, etc.

Recently there has been enormous interest in the research and development of microfluidics because of increasing demands from biological applications such as genomics, proteomics, and drug

discovery. Therefore, an important direction in the development of analytical techniques is toward microanalyzer, Generic names for these new micrometer-featured devices include “micro- total analysis systems” ($\mu$-TAS) (Manz *et al*., 1990) [2], lab-on-a-chip (Colyer *et al*.,1997； Moser *et al*.,1995), biochip, or, simply “chip.” A promising analytical tool for analyzing proteins and protein complexes in the biology laboratory of the future is a microfluidic device. These "laboratories" (as the Fig.1) are fabricated using photolithographic processes developed in the microelectronics industry to create circuits of tiny chambers and channels in a quartz, silica, or glass chip. They direct the flow of liquid chemical reagents just as semiconductors direct the flow of electrons. These reagents can be diluted, mixed, reacted with other reagents, or separated — all on a single chip. In some cases devices have been named based on their particular application, for example, PCR chip [4], gene chip, while for others the device is named for characteristic structure feature, for example, microspot or microarray. The drug delivery microsystem consists of micropumps, biosensors, flow sensors, microvalves, microreservoirs, microneedles, and a feedback controller.

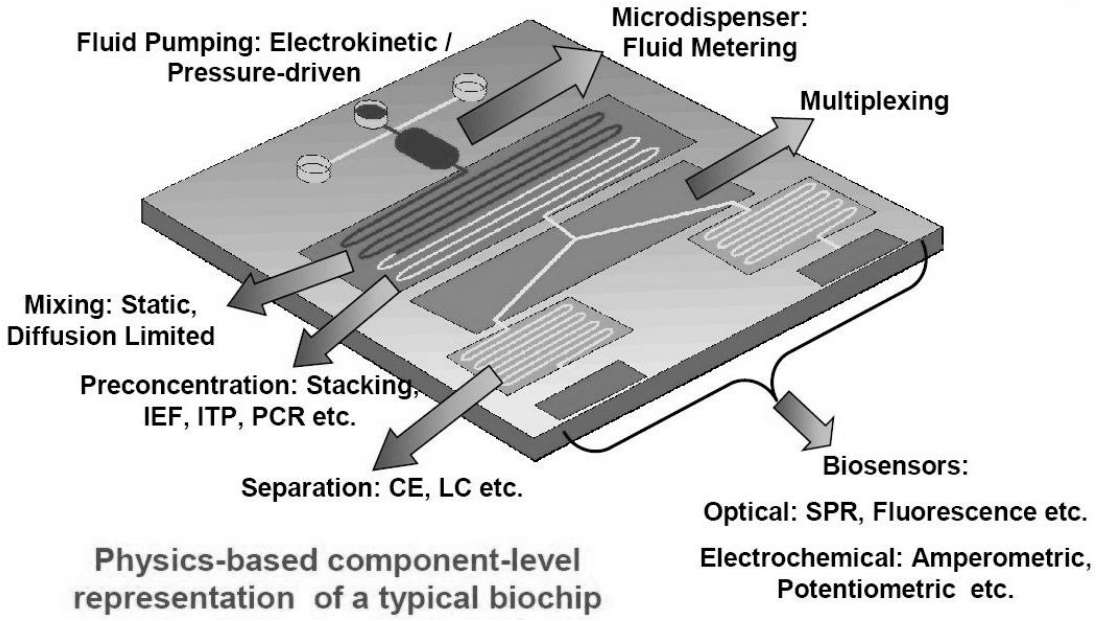


Fig. 1 A Typical Biochip Layout—Component [3]

Micropump is one of the MEMS devices, which can be used for drug delivery applications. It provides the driving force to mobilize fluids in the system, which then enables functions such as mixing, reaction, injection, and separation, in other words, this device as the main part of a drug delivery system transfers the fluid (drug) from the drug reservoir to the body (tissue or blood vessel) with high performance, accuracy, and reliability. Most drugs have a range of concentrations of greatest efficacy in the body, above which they are toxic and below which they have no therapeutic benefit [5].Conventional drug delivery routes such as oral tablets or injections are not easily able to control the rate of drug delivery or the target area of the drug. Consequently, initial concentration of the drug in the blood peaks above the level of toxicity and then gradually decreases over time to an ineffective level and the patients

have to take the drug frequently. In order to control drug release better, drug delivery systems (DDS) are necessary. Small size and high precision of micropumps have made them useful for chemotherapy, insulin delivery for diabetic patient, and drug dosing for cancer patient and so on [6].

## 1.2 Literature Review

Research on micropumps has been popular among MEMS scientists for more than 20 years [7–11]. In the first years of research this popularity may have been caused by the fascinating fact that these tiny devices produce fluid motion that is visible to the naked eye. Now more and more applications drive researchers to improve their micropumps. Most micropumps found today can roughly be divided into two groups [12]:

"Continuous flow micropumps" are based on a direct transformation of nonmechanical or mechanical energy into a continuous fluid movement. While mechanical pumping was mostly used in macroscale pumps and micropumps with a relatively large size and high flow rates, this second category discovers its advantages in the microscope. Since the viscous force in microchannels increases in the second order with miniaturization, the first pump category can not deliver enough power to overcome the high fluidic impedance in the microscale.

Mechanical pumps can be further categorized according to the

principles by which mechanical energy is applied to the fluid. Under this system, mechanical pumps are divided into two major categories: displacement pumps and dynamic pumps.

In displacement pumps, energy is periodically added by the application of force to one or more moveable boundaries of any desired number of enclosed, fluid-containing volumes, resulting in a direct increase in pressure up to the value required moving the fluid through check valves or ports into the discharge line. Check-valve pumps, peristaltic pumps, valve-less rectification pumps, and rotary pumps belong to the displacement category.

In dynamic pumps, mechanical energy is continuously added to increase the fluid velocities within the machine. The higher velocity at the pump outlet increases the pressure. Centrifugal pumps and ultrasonic pumps belong to the dynamic category. (Table 1)

Table 1 Mechanical pumping principles

| *Displacement Pumps* | *Dynamic Pumps* |
|---|---|
| • Check-valve pumps | • Ultrasonic pumps |
| • Peristaltic pumps | • Centrifugal pumps |
| • Valve-less rectification pumps | |
| • Rotary pumps | |
| • Tesla type valves | |

The so-called “displacement pumps or reciprocating micropumps” use the oscillatory or rotational movement of mechanical parts to

displace fluid. Micropump development has started with “piston type” reciprocating micropumps like micro diaphragm pumps and peristaltic micropumps that do still form the main representatives of this class in the MEMS world. Mechanical pumps can handle a large variety of fluids, but often involve complicated structures and present integration challenges, as is evident in rotary pumps [13] (requiring bearings) and some diaphragm pumps requiring check valves [14](it function under conditions of a small compression ratio and of high pump pressure), diffuser/nozzle [15] (or valveless rectification micropump) pumps (as Fig.2) Besides, a Tesla [16] Type Valve (as Fig.3) is one of the no-moving parts (NMP) type valves used in micropumps for Micro Electro Mechanical System (MEMS) devices. This pump type can be realized easily in silicon with DRIE technology. Its principle of operation is based on the rectification of the fluid flow. For the same pressure drop, the flow in the forward direction through the valve is greater than the flow in the reverse direction, thus if an oscillating flow field can be set up, there should be net mass flow in the forward direction.

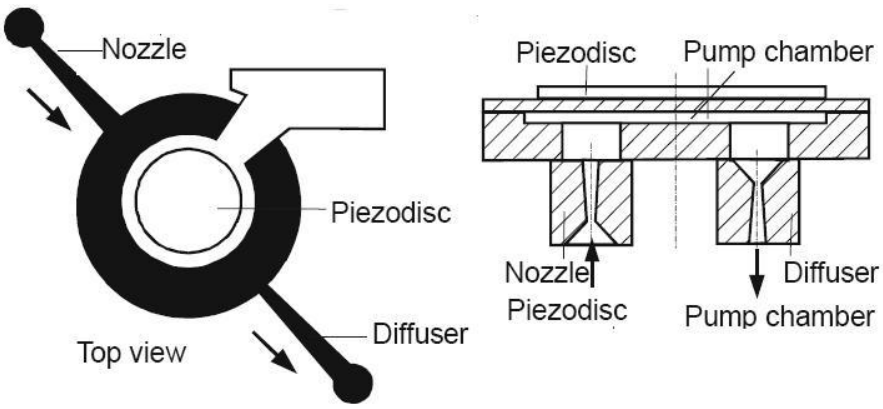

Fig. 2 valveless rectification micropumps

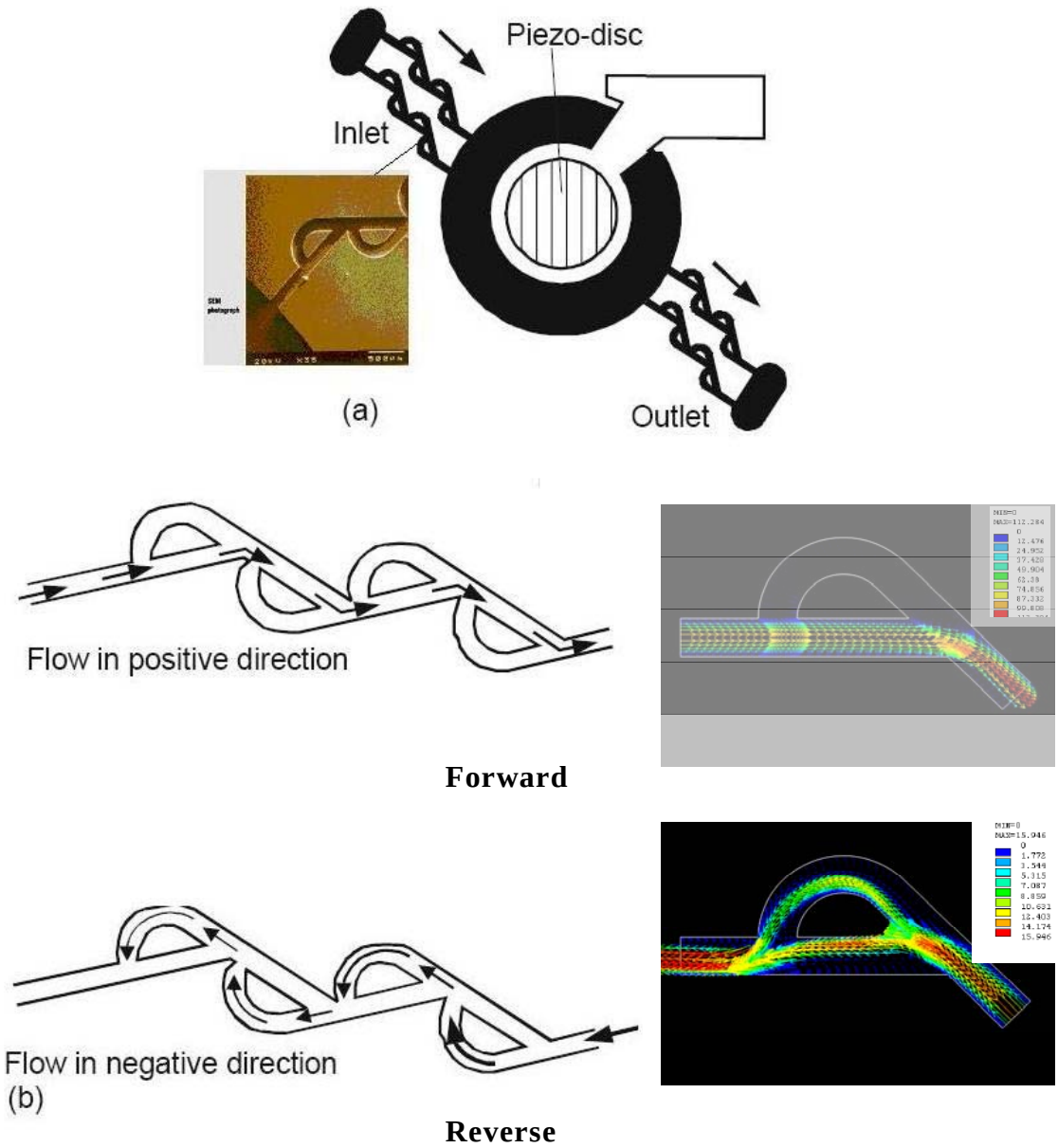


Fig. 3 Tesla pump: (a) design example; and (b) rectification effect

In addition, different methods of actuation have been applied to micropumps such as electrostatic actuators, piezoelectric actuators,

magnetohydro- dynamic, shape memory alloy actuators, and thermal actuators. However, most of them have complex structures and are difficult to be miniaturized. Furthermore, their output power is limited and not sufficient for practical applications. Piezoelectric actuators are most promising, nevertheless, owing to their simple structure, and great output power density. Van Lintel is the first person who used a piezoelectric disc glued to a glass membrane [17]. Under a voltage difference the piezoelectric disc changes its lateral dimension which results in a bending moment in the dimorph. The original prototype was able to produce a maximum pressure of 100 cm water and a maximum yield of 10 μl/min at 1 Hz block wave actuation. Figure 4 illustrates the typical flow rate range of micropumps. For flow rates more than 10 ml/min, miniature pumps or macroscale pumps are the most common solutions. The typical operation range of displacement micropumps lies between 10 μl/min and several milliliters per minute. For flow rates less than 10 μl/min, alternative dynamic pumps or nonmechanical pumps are needed for an accurate control of these small fluid amounts.

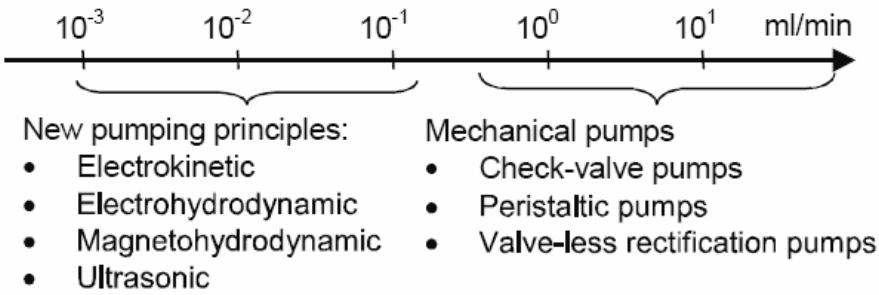


Fig. 4 Flow rate range of different pump principles.

There are many groups now active in the design of micropump. A simple analytic model is presented to optimize the valveless diffuser pump by Olsson *et al* [18-19] and Ullmann [20] analyzed the performances of single and double chamber micropumps and discussed the dependence of the flux on pressure difference between the inlet and the outlet.

Pan *et al* [21] investigated the mechanical properties of fluid–membrane coupling for a valveless micropump, but the unsteadiness of the flow field within the micropump was not accounted for in their investigation. Two years further on, the inertial effects [22] was presented to shows that a phase shift lagging the excitation force exists in the vibration response. The dynamic response of a cantilever is investigated to find the connections between the nature frequency and structure by Naik [23]. Kan [24] expounds the concept of dynamic response into piezoelectric cantilever-valve micropumps. The analysis results suggest that check efficiency of cantilever valve depends on phase shift, which increases with the increasing of driving frequency. Several authors have considered low-order or "electrical-equivalent" models for micropumps.

Among all kinds of pumps, peristaltic pumps have many advantages for biomedical applications. First of all, the peristaltic micropump doesn't have a moving part. The main advantage of the peristaltic pump is that no seals, valves or other internal parts ever touch the fluid. Due to the simplicity of their structures, peristaltic

pumps have found many applications in the pharmaceutical, chemical, and food industries. Besides this, the action of a peristaltic pump is very gentle, which is important if the fluid is easily damaged. Therefore, the particles and living cells would not be stuck or damaged. The risk of clogging in the channels is also reduced, as a result. Secondly, the pump could be operated in the forward and backward directions. Furthermore, it doesn't have passive check valves as flow directing elements that open and close frequently; therefore, the valves will not easily be worn out and cause mechanical fatigue. In other words, peristaltic pumps are good for long-term treatments. Especially, it is suitable for reagents and cells pumping. Finally, the planar design is less complex with high pump performance, and has the ability to pump a wide variety of fluids.

B Husband [25] presents the peristaltic micropump with three PZT actuated glass membranes and silicon channels, is integrated within the $\mu$TAS device with microfluidic reaction chambers.

## 1.3 Working Principle and Performance for a Peristaltic Micropump

In contrast to diffuser/nozzle pumps, peristaltic pumps synchronize several piezo discs in a wave-like motion. This peristaltic motion transports the fluids in one direction and requires no diffuser/nozzle. Classical peristaltic pumps generate the

wave-like motion by a wheel with roles along the circumference. The roles press on a flexible silicon rubber tube and cause the wave-like motion when the wheel rotates [26].

In our design, the basic elements of the peristaltic micropump consist of three chambers, and to operate in a peristaltic motion by the driving circuit. The driving circuit actuates the PZT to produce the pressure on the diaphragm with oscillating motion. The common driving scheme of a peristaltic micropump was divided into six phases (100, 110, 010, 011, 001, and 000) as depicted in Fig. 1. In phases 1 to 3 fluids was drawn into the pump chamber through the inlet valve, which is then displaced through outlet valve in phases 4 to 6. Thus one circle is complete. To repeat in circles, make the pump achieve self priming.

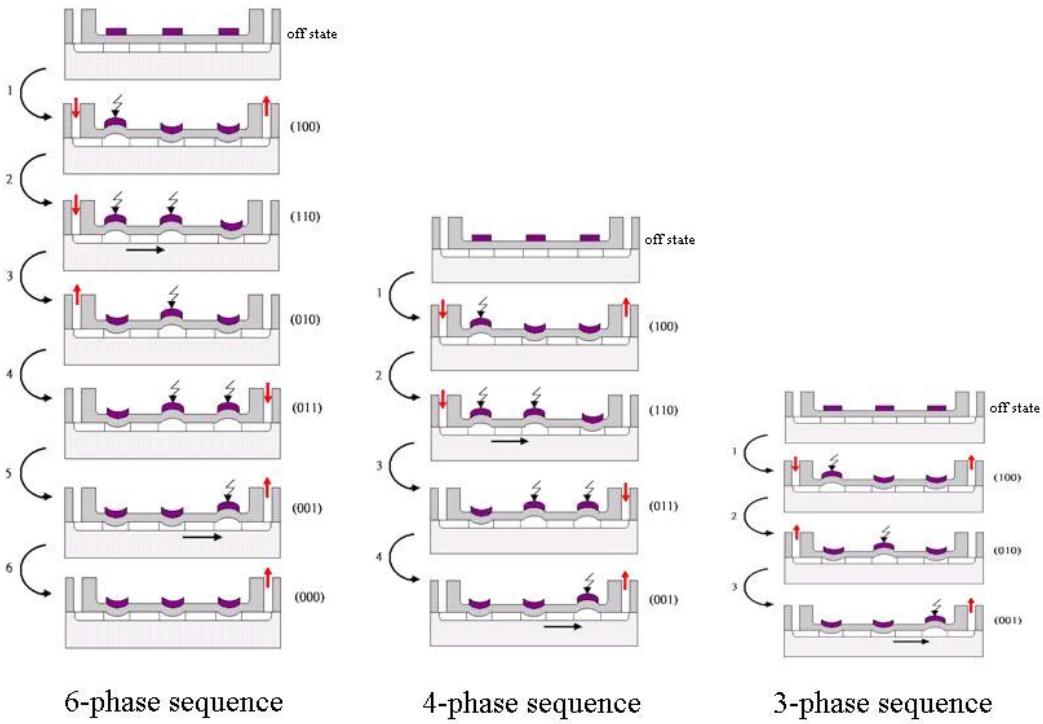

Fig. 5 Actuation sequences of a peristaltic micropump based on piezoelectric actuation micropump

Below is a series of six-phase diagrams illustrating

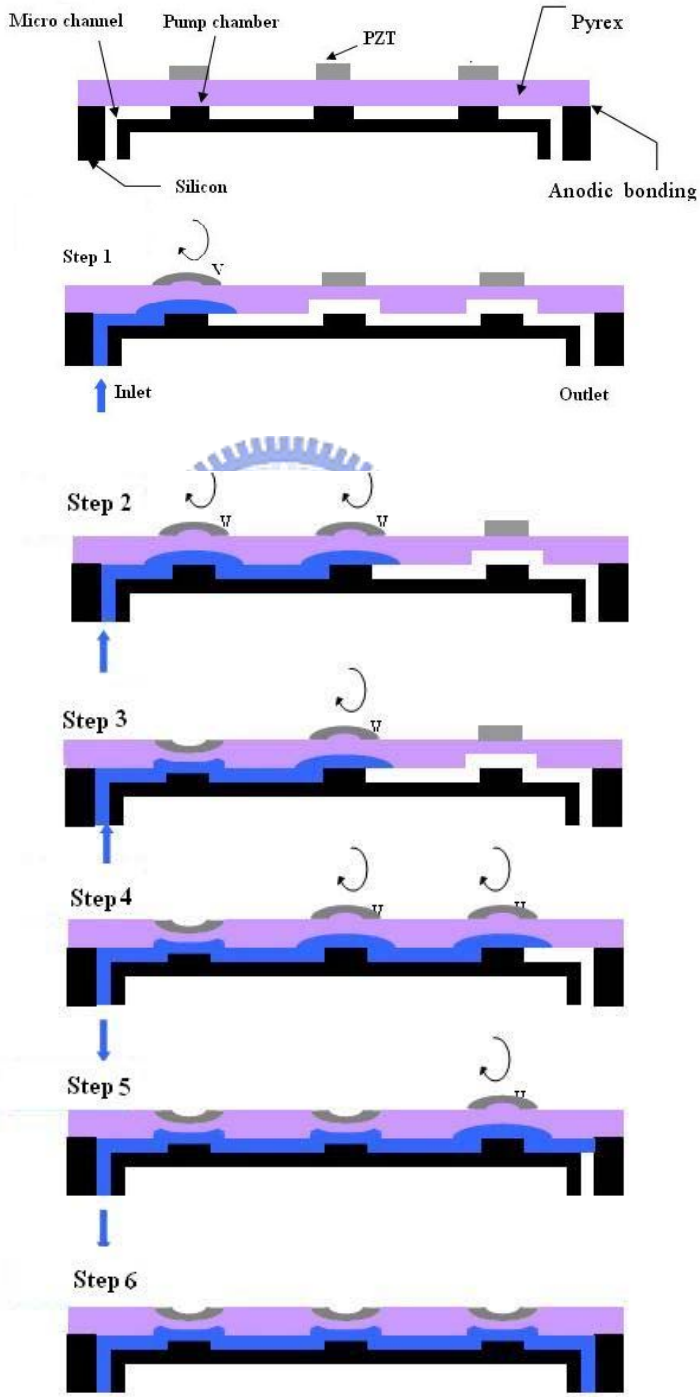

Fig. 6 The flow chart of a six-phase driving peristaltic micropump

The driving scheme of the four-phase mode (100, 110, 011, and 001) was the six-phase scheme that removes the process of phases 3 and 6. By the same way, the driving scheme of the 3-phase (100, 010, 001) was the six phase scheme that removes the process of phases 2, 4 and 6.

# CHAPTER 2
# THE DAMPING EFFECTS ON THE MICRO-DIAPHRAGM

## 2.1 Piezoelectric Materials

The piezoelectric force has been widely used for micromechanical devices. The effect was discovered by Jacques and Pierre Curie in 1880. They discovered that if special crystals were subject to mechanical tension, they became electrically polarized and the polarization was proportional to the extension. They also discovered that the opposite was true; if an electrical field was applied across the material it deformed. This is known as the inverse piezoelectric effect. Piezoelectricity involves the interaction between the electrical and mechanical behavior of the medium. To the first order this is described as [27]

$$\{S(T,E)\}_{6\times1} = s^{E}_{6\times6}T_{6\times1} + d_{6\times3}E_{3\times1} \qquad (2\text{-}1)$$

where ***S*** is the strain, $s^{E}$ is the compliance tensor under conditions of constant electric field, ***T*** is the stress, *d* is the piezoelectric charge constant tensor and ***E*** is the electric field. The deformation of a piezoelectric crystal is illustrated in Fig. 6 In the absence of mechanical loads Eq. (2-1) gives

$$\Delta l = d_{33} \cdot U = d_{33} \cdot \frac{U}{l} \cdot l = d_{33} \cdot E \cdot l \tag{2-2}$$

And

$$\Delta a = d_{31} \cdot U = d_{31} \cdot \frac{U}{l} \cdot a = d_{31} \cdot E \cdot a \tag{2-3}$$

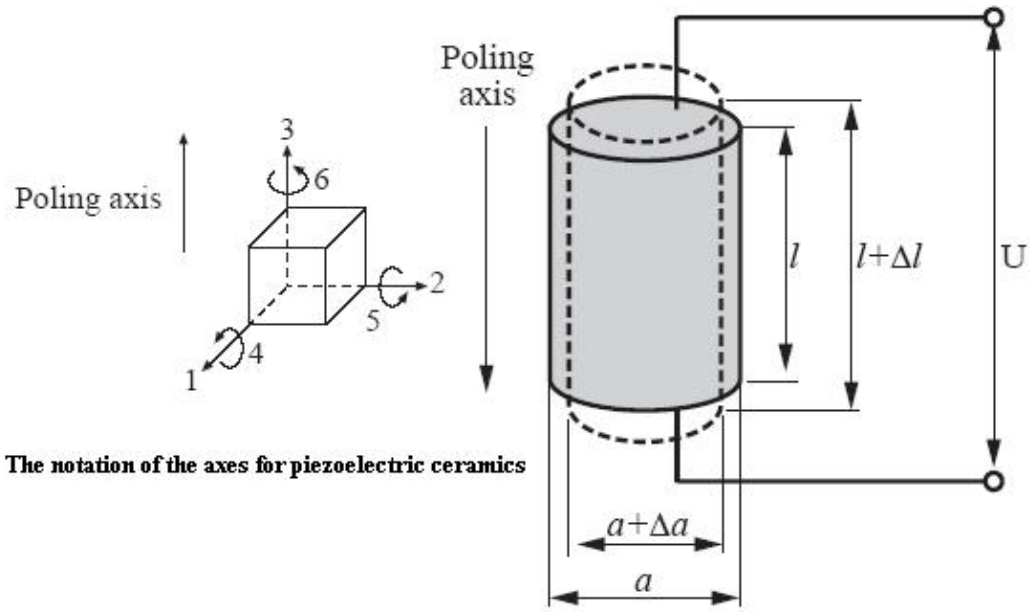


Fig. 7 The deformation of a piezoelectric device when subject to an electrical voltage

where $\Delta l$ is elongation along the poling axis, $l$ is the device length along the poling axis, $U$ is the electrical voltage, $\Delta a$ is elongation perpendicular the poling axis and $a$ is the device length perpendicular to the poling axis. Normally $d_{33}$ >0 and $d_{31}$ < 0.

Examples of piezoelectric materials are quartz, LiTaO3, PZT and ZnO. Non-piezoelectric materials, e.g. silicon, can be exited by

depositing a thin film of a piezoelectric material, e.g. PZT or ZnO. Another solution is to mount a piezoelectric disk on the non-piezoelectric material. This eliminates the problem of making the film thick enough that high voltages can be applied without dielectric breakdown (sparks/short circuits across the film). The piezoelectric effect can be used to bend a diaphragm, e.g. in a pump. The principle is illustrated in Fig. 7 where a piezoelectric disk is glued to a diaphragm. When a voltage is applied across the piezoelectric disc it deforms and forces the diaphragm to bend.

## 2.2 Performance of the Frequency-dependent Flow Rate

Small vibrational structures, typically in the shape of diaphragm、beam and plate at the micron scale fabricated by silicon technology, have received ever increasing interest because they can be used as key components in developing sophisticated microelectromechanical systems (MEMS) including microsensors and actuators.

In this section we will examine the responses of single-degree of–freedom systems. This is one of the most important topics to master, since the more complicated cases can be treated as if they are simply collections of a spring-mass system. Now, I would like to focus attention on one of the chambers in the peristaltic micropump for the sake of a simplification. With a micropump, the release rate of drug delivery is able to be controlled easily to maintain the

therapeutic efficacy. Hence, with taking into account the influence of liquid added mass and added damping on the dynamic characteristics of the micro diaphragm and actuator in the natural frequency, a performance of piezoelectric micropump was investigated for this purpose.

If a statically or periodically loaded elastic system, such as a spring、beam or membrane, is disturbed in some manner from its position of equilibrium, the internal forces and moments in the deformed configuration will no longer be in balance with the external loads and vibrations will occur. In the piezoelectric micropump, the fluid flow is driven by the vibrating actuator. At the same time, the fluid plays a key role in resistance to the actuator vibration. The actuator vibration, the micro-diaphragm movement and the fluid flow are thus coupled. The fluid reaction force is represented as an added mass and added damping contribution to the dynamic response of the structure without affecting their stiffness. The added mass and added damping depends on both the fluid density and viscosity, as well as on the gap height in the chamber and a solid surface. Therefore with fluid (e.g. air, water or blood) as the pump medium, the dynamical behaviors of the actuator and the micro-diaphragm are different from those in vacuum.

### 2.2.1 A Simple Spring-mass-damper System under Simple Harmonic Excitation

The basic element in the micro-diaphragm pump is shown in Fig. 9. Therefore, very simplified, this can be seen as a Helmholtz resonator or as a mass-spring system. We define the bi-layer "piezoelectric disk and Pyrex glass diaphragm" as the micro-diaphragm. In this case, the spring is the micro-diaphragm. Such a system is illustrated in Fig. 8 where also viscous damping is included. $f_e$ is the periodic actuating force and $P$ is the dynamic pressure exerted on the diaphragm by the liquid. Clearly, undamped systems are not highly accurate models of the real world (especially for high viscosity fluid) since we know that the unforced oscillations of real systems always decay away eventually. Like all systems possessing mass and elasticity it is capable of free vibration, i.e. it has natural frequencies. When such a system is subject to harmonic excitation it is forced to vibrate at the same frequency as the excitation frequency. When a system is excited by a transient force, the resulting excitation take place at the natural frequencies of the system with the amplitude varying depending on the excitation.

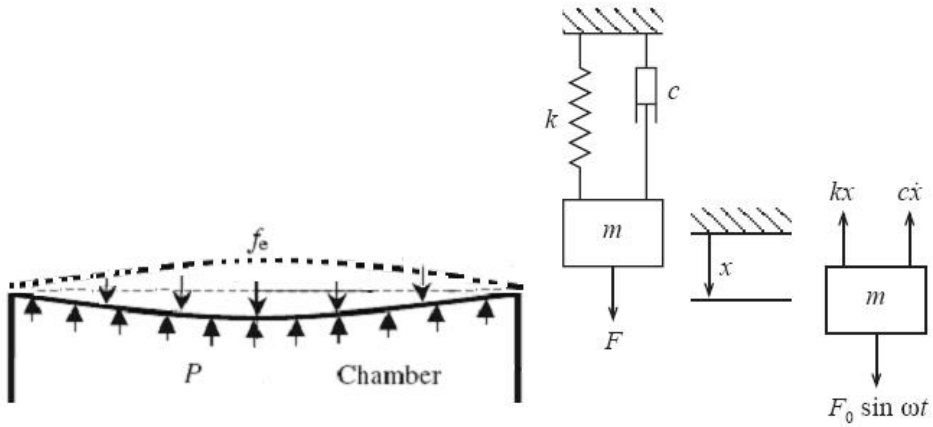


Fig. 8 A simplified diaphragm micropump viscously damped system with harmonic excitation.

In consideration of the liquid added mass and added damping, the dynamic equation of a damping driven harmonic oscillation of the micro-diaphragm can be expressed as

$$m\ddot{x} + c\dot{x} + kx = f(t) \tag{2.4}$$

Dividing by m, as we did for solving ordinary differential equation

$$\ddot{x} + \frac{c}{m}\dot{x} + \frac{k}{m}x = f(t) \tag{2.5}$$

The parameters $m$, $c$, $k$ and $F$ stand for the total effective mass of the micro-diaphragm in liquid environment ($M$=$M_v$ +$M_{ad}$ ,$M_v$ is the mass of the micro-diaphragm and $M_{ad}$ is the adding mass of liquid), the added damping constant, the spring constant of the micro-diaphragm and the driving force provided by the piezoelectric actuator, respectively. We next assume that our forcing is sinusoidal and introduce the notations ： $w_n^2 = \frac{k}{m}$, $\zeta = \frac{c}{2\sqrt{mk}}$

we obtain

$$\ddot{x} + 2\zeta w_n \dot{x} + w_n^2 x = \frac{\bar{f}}{m}\sin(wt) \tag{2.6}$$

which is the differential equation of motion for forced vibrations with viscous damping. A particular solution of Eq. (2.3) can be taken in the form (2.4) because we realize that sines and cosines are linearly independent functions； there is no way to get one from the other.

$$x = M\cos wt + N\sin wt \tag{2.7}$$

where $M$ and $N$ are constants. To determine these constants, we use operator to solve it

$(a_n D^n + a_{n-1}D^{n-1} + \cdots + a_1 D + a_0)x = r(t)$, namely $L(D)x = r(t)$

$$(D^2 + 2\zeta w_n D + w_n^2)x = \frac{\bar{f}}{m}\sin(wt) \tag{2.8}$$

$$x(t) = I_m\left[\frac{1}{D^2 + 2\zeta w_n D + w_n^2}\frac{\bar{f}}{m}e^{iwt}\right]$$

$$\Rightarrow x(t) = I_m\left[e^{iwt}\frac{1}{(iw)^2 + i2\zeta w_n w + w_n^2}\frac{\bar{f}}{m}\right]$$

$$x(t) = I_m\left[\frac{\cos wt + i\sin wt}{(w_n^2 - w^2) + i2\zeta w_n w}\frac{\bar{f}}{m}\right]$$

Upon multiplying both numerator and denominator by the term $(w_n^2 - w^2) - i2\zeta w_n w$

$$x(t) = I_m\left\{\frac{(\cos wt + i\sin wt)\left[(w_n^2 - w^2) - i2\zeta w_n w\right]}{(w_n^2 - w^2)^2 + (2\zeta w_n w)^2}\right\}$$

Taking the imaginary part of $x(t)$, we obtain

$$x(t) = -\frac{(2\zeta w_n w)\frac{\bar{f}}{m}}{(w_n^2 - w^2)^2 + (2\zeta w_n w)^2}\cos wt + \frac{(w_n^2 - w^2)\frac{\bar{f}}{m}}{(w_n^2 - w^2)^2 + (2\zeta w_n w)^2}\sin wt \qquad (2.9)$$

Thus, $M$ and $N$ are：

$$M = -\frac{(2\zeta w_n w)\frac{\bar{f}}{m}}{(w_n^2 - w^2)^2 + (2\zeta w_n w)^2} \quad \text{and} \quad N = \frac{(w_n^2 - w^2)\frac{\bar{f}}{m}}{(w_n^2 - w^2)^2 + (2\zeta w_n w)^2} \qquad (2.10)$$

Only $N$ can ever equal zero and this occurs only if the forcing frequency is equal to the system's natural frequency. At all frequencies $M$ is nonzero, and hence we always will have some finite response. The total solution of Eq. (2.6) is obtained by adding the general solution to the particular solution (2.9)

$$x(t) = c_1 \exp\left[(-\zeta + \sqrt{\zeta^2 - 1})w_n t\right] + c_2 \exp\left[(-\zeta - \sqrt{\zeta^2 - 1})w_n t\right]$$
$$+ \frac{-(2\zeta w_n w)\frac{\bar{f}}{m}}{(w_n^2 - w^2)^2 + (2\zeta w_n w)^2}\cos wt + \frac{(w_n^2 - w^2)\frac{\bar{f}}{m}}{(w_n^2 - w^2)^2 + (2\zeta w_n w)^2}\sin wt \qquad (2.11)$$

The first two terms in Eq. (2.11) represent damped free vibrations, that due to the factor $e^{-nt}$ the free vibrations gradually subside, leaving only the steady forced vibrations represented by the last two terms. These forced vibrations are maintained indefinitely by the action of the disturbing force from the excitation of PZT actuators and, therefore, are of great practical importance. We shall now see how they affected by damping.

We'll use the trigonometric formula：

$$\sin(a - b) = \sin(a)\cos(b) - \cos(a)\sin(b)$$

$$M \cos wt + N \sin wt = A_d \left[\sin(wt)\cos\phi - \cos(wt)\sin\phi\right]$$

$$A_d = \sqrt{M^2 + N^2} \quad \text{and} \quad \phi = -\tan^{-1}(\frac{a}{b})$$

The steady-state response Eq. (2.9) may be written in the equivalent phase angle form as

$$x(t) = A_d \sin(wt - \phi) \tag{2.12}$$

from which, and substituting the actual values of $M$ and $N$

$$\phi = \tan^{-1}(\frac{2\zeta w w_n}{w_n^2 - w^2}) \tag{2.13}$$

and

$$A_d = \frac{\bar{f}}{m} \frac{1}{\sqrt{(w_n^2 - w^2)^2 + (2\zeta w_n w)^2}} \tag{2.14}$$

In this case $\phi$ has a physical meaning, that is, the amount that the output lags the input.

Introducing the nondimensional frequency: $\Omega = \frac{w}{w_n}$

$$\phi = \tan^{-1}(\frac{2\zeta\Omega}{1 - \Omega^2}) \tag{2.15}$$

and

$$A_d = \frac{\bar{f}}{m} \frac{1}{\sqrt{(1 - \Omega^2)^2 + (2\zeta\Omega)^2}} \tag{2.16}$$

### 2.2.2 Complex Representations

Although representing a system's response as Eq. (2.7) is physically attractive, it is a bit awkward mathematically. Our

solution to this problem will be to represent $x(t)$ as complex notation, namely

$$\ddot{x} + 2\zeta w_n \dot{x} + w_n^2 x = \frac{\bar{f}}{m} e^{iwt} \tag{2.17}$$

The steady-state solution is given by

$$x = \bar{x} e^{iwt} \quad \text{, and} \quad \bar{x} = \frac{\bar{f}}{m} \frac{1}{(w_n^2 - w^2) + 2i\zeta w w_n}$$

in terms of mass $m$, spring $k$ constant and damping constant $c$, respectively

$$\bar{x} = \frac{\bar{f}}{k} \frac{1}{1 - \frac{m^2}{k^2} w^2 + i \frac{c}{k} w} \tag{2.18}$$

## 2.3 Analysis of the Simplified Micropump for the Flow Rate

The diaphragm structure acts as a “piston” which transfers energy to the fluid in the pump chamber, when driving voltage is sine wave, in one period, the fluid flows into the pump chamber in [0, T/4] and [3T/4, T]. The fluid flows out the pump chamber in [T/4, 3T/4]. So it is just necessary to calculate the flow rate in [T/4, 3T/4]. The Mach number is the ratio between the flow velocity $u$ and the speed of sound $a$ and is given by:

$$M_a = \frac{V}{a} \tag{2.19}$$

The Mach number is a measure of the compressibility of a gas and can be thought of as the ratio of inertial forces to elastic forces. For the Mach-number in the pump chamber is approximately 5.25e-5 (less than 0.3). Under the conditions the density of a gas will not change significantly while it is flowing through a system. The flow is then considered to be incompressible even though fluid, a gas, is still considered compressible. The compression could be neglected when calculating the pump's flow rate. The analysis of an incompressible gas flow is greatly simplified as it can be treated with the same versions of the governing equations that will be derived for liquid flows.

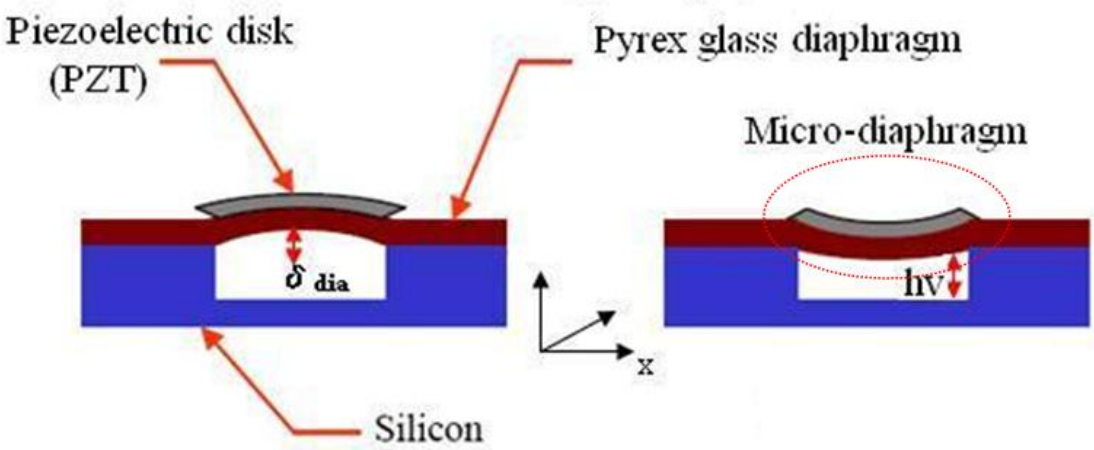


Fig. 9 The schematic of a diaphragm micropump for analysis of flow rate

Assume $h_v$ is the distance between diaphragm and the bottom of pump chamber as the figure 9. It could be expressed as[28]：

$$h_v = h' + \delta_{dia} \sin 2\pi wt \qquad (2.20)$$

where $\delta_{\mathrm{dia}}$ is the centerline displacement of the interior surface of the membrane, i.e. the vibration amplitude； $h'$ is the diaphragm's original distance between diaphragm and pump chamber's bottom surface； $w$ is vibration frequency

Introducing a parameter to correct Eq. (2.20), The membrane shape factor $\gamma$： it was also determined based on the static membrane displacement ：

$$\gamma = \frac{v}{A_c \delta_{dia}} \qquad (2.21)$$

where $v$ is the volume swept out by the membrane, $A_c$ is the area of the chamber

Not considering the compression and leakage, the instantaneous volume ($V$) of the pump chamber in [T/4，3T/4] is:

$$V = (h' + \gamma \delta_{dia} \sin 2\pi wt) BL \qquad (2.22)$$

where $L$ and $B$ is the length and width of the pump chamber. The change ratio of the instantaneous volume is equal to the instantaneous flow $Q$, we have:

$$Q = V' = 2\pi w \gamma BL \delta_{dia} \cos 2\pi wt \qquad (2.23)$$

As we known, the pump's instantaneous flow also could be expressed as:

$$Q = 2AV$$

$$A = Bh = B(h' + \gamma\delta_{dia}\sin 2\pi wt) \qquad (2.24)$$

where $A$ and $v$ are the instantaneous micro-diaphragm and chamber cross-section area and the flow rate in pump chamber length direction (x direction), respectively; From the eq. (2.23), and eq. (2.24), we have:

$$v = \frac{Q}{2A} = \frac{\delta_{dia}\,\gamma L\pi w \cdot \cos 2\pi wt}{h' + \gamma\delta_{dia}\sin 2\pi wt} \qquad (2.25)$$

Thus, the mean flow rate $\bar{v}$ is:

$$\bar{v} = \frac{\int_{1T/4}^{3T/4} v\,dt}{T} = \frac{\pi w}{T}\int_{1T/4}^{3T/4} \frac{\delta_{dia}\,L \cdot \gamma\cos 2\pi wt}{h' + \gamma\delta_{dia}\sin 2\pi wt}\,dt \qquad (2.26)$$

The eq. (2.26) can be simplified to:

$$\bar{v} = \frac{L}{2T}\ln\frac{h' - \gamma\delta_{dia}}{h' + \gamma\delta_{dia}} \qquad (2.27)$$

Assume $\eta$ is leakage factor, the mean flow rate considered the leakage is as follow:

$$\bar{v} = \eta\frac{L}{2T}\ln\frac{h' - \gamma\delta_{dia}}{h' + \gamma\delta_{dia}} \qquad (2.28)$$

The fundamental relation for the piezo effect will be described by the following equation:

$$\frac{\Delta l}{l} = sT + d_{31}\frac{U}{t} \qquad (2.29)$$

Here $\Delta l/l$ is the relative expansion of the piezoelectric material achieved by applying a voltage $U$ between the diaphragm and the upper-electrode (t: thickness of the piezo ceramic). The

electromechanical ransformation depends on the piezoelectrical coefficient of the ceramic material, described by $d_{31}$, on the stiffness $s$ and on the mechanical load $T$

This is especially noteworthy in the case of a combination of a rectangular piezo disk and rectangular Pyrex glass diaphragm, the load T cannot be deduced by analytic equations. For a approach, the calculation of the pump diaphragm displacement is possible assuming circular plates with a radius $R_p$ instead of square plates for the diaphragm and piezo disk. As an essential result of this model the deflection $w(r)$ of the pump diaphragm can be calculated by

$$w(r) = -\frac{3d_{31}U}{t_b^2} R_p^2 \left(1 - \frac{r^2}{R_p^2}\right) \tag{2.30}$$

For $r$=0 the maximal deflection $w(r)$ can be calculated to

$$w(r=0) = w_{\max} = -\frac{3d_{31}U}{t_b^2} R_p^2 \tag{2.31}$$

From the Eq. (2.16), (2.29) and (2.31), the diaphragm's amplitude could be expressed as

$$\delta_{dia} = \frac{3l^2 d_{31} U}{t_b \sqrt{\left(1 - \frac{w^2}{w_0^2}\right)^2 + \left(2\zeta \frac{w}{w_0}\right)^2}} \tag{2.32}$$

Substitute Eq.(2.32) and $f$=1/$T$ into Eq.(2.28):

$$\bar{v} = \frac{Lw\eta}{2} \ln \frac{h' t_b^2 \sqrt{\left(1 - \frac{w^2}{w_0^2}\right)^2 + \left(2\zeta \frac{w}{w_0}\right)^2} - \gamma 3 l^2 d_{31} U}{h' t_b^2 \sqrt{\left(1 - \frac{w^2}{w_0^2}\right)^2 + \left(2\zeta \frac{w}{w_0}\right)^2} + \gamma 3 l^2 d_{31} U} \tag{2.33}$$

This is the expression of the diaphragm pump's mean flow rate which relates with the amplitude and frequency of the voltage, pump's chamber length, bimorph's parameters, leakage factor, the membrane shape factor etc..

## 2.4 The Added Mass and Added Damping

A primary concern in the design of the peristaltic micropump is damping effects on the frequency response. In certain simplification cases, the vibration problems can be reduced to the case of a system with one degree of freedom. In addition, the mass of the spring, beam or membrane can be neglected in comparison with the mass of the load weight $W$. In our case, therefore, we can regard the load weight $W$ as excitation force from the piezoceramic, PZT. Although these simplifications are accurate enough in many practical cases, there are technical problems in which a detailed consideration of the accuracy of such approximation becomes necessary. With the miniaturization of the size (range of $\mu m$ to $mm$) in the microelectromechanical systems (MEMS) technology, the analysis of vibration and damping play important role in mechanical

engineering design. When a micro-diaphragm vibrates in a viscous fluid, the fluid offers resistance to the motion of the diaphragm. The fluid loading can be interpreted as the sum of two forces: an inertial force that is proportional to the acceleration of the diaphragm (the proportionality constant is called added mass), and a viscous or dissipative force that is proportional to the velocity of the diaphragm (the proportionality constant is called added damping or viscous damping coefficient).

In order to determine the effect of such simplification on the frequency of vibration, an approximate method developed by Lord Rayleigh will now be discussed. In applying this method some assumption regarding the configuration of the system during vibration must be made. The frequency of vibration will then be from a consideration of the conservation of energy in the system.

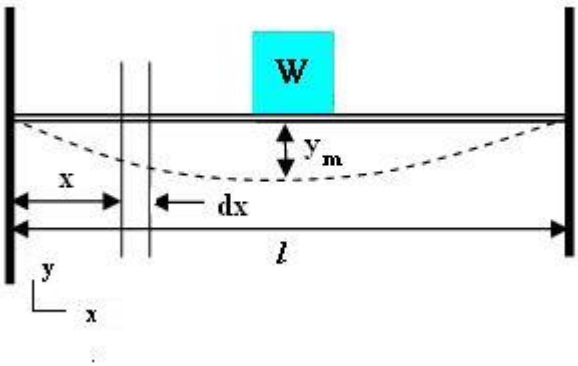


Fig. 10 vibration of a beam of uniform cross section loaded at the middle with a block of weight W

Let $w$ denote the weight of the spring per unit length. If the weight

$wl$ of the beam is small in comparison with the load W，it can be assumed with sufficient accuracy that the deflection curve of the beam during vibration has the same shape as the static deflection curve for a concentrated load at the middle. $y_m$ is the displacement at the center of the beam (see Fig.10) and we express the displacement of any element located at s distance x from the support as :

$$y = y_m \left(\frac{3xl^2 - 4x^3}{l^3}\right)$$

The maximum kinetic energy of the beam itself will be

$$2\int_0^{l/2} \frac{w}{2g}\left(\dot{y}_m \frac{3xl^2 - 4x^3}{l^3}\right)^2 dx = \frac{17}{35} wl \frac{\dot{y}_m^2}{2g}$$

This kinetic energy of the vibrating beam must be added to the energy $W\dot{y}_m^2 / 2g$ of the loaded concentrated at the middle in order to estimate the effect of the weight of the beam on the period of vibration. In this case the period of vibration will be the same as for a massless beam loaded at the middle at the middle by the weight

$$W' = W + \frac{17}{35} wl \tag{2.34}$$

Considering a homogeneous beam, which is vibrating in liquid, has thickness $h$, length $L$, width $B$, mass density $\rho_d$ and the mass per unit length $m_d = hb\rho_d$. In such a simple model, the added mass and added damping per unit length of the beam are roughly:

$m_{ad} = \frac{\rho B^3}{10h_0}, c = \frac{\mu B^3}{h_0^3}$ with $\rho$ and $\mu$ standing for the liquid density and the liquid dynamic viscosity, respectively.

$$M = \frac{17L}{35}(m_d + m_{ad}), C = 12\pi Lc$$

## 2.5 Analysis of the Frequency Shift with the interactions exerted on the micro-diaphragm

With a micropump, such diaphragm structure acts as a "piston" to provide power for the handling of microliter-scaled fluid volumes desired in many lab-on-a-chip chemical and biomedical applications. In the design of the mechanical efficiency, the pump performance hangs on using resonance to generate sufficient motion of the diaphragm. We are concerned with the interactions between a system and its environment (such as the implicit pressure and shear stress at the solid-fluid interface and the force exerted by the PZT actuator) for the influence on output resonance frequency.

The micro-diaphragm (the Piezoelectric disk and Pyrex diaphragm bi-layer) is integrated with surrounding walls; therefore, it can be considered as a flexible double-clamped beam spring-mass-damper system (as Fig.8). However, the various working fluids play different roles in resistance to the diaphragm vibration. Many inputs to physical systems are periodic in nature. For example, the forces exerted on marine structures by ocean

waves, the acoustic and electric waveforms of music and speech and mechanical vibrations exerted on structures due to unbalanced elements are all inherently cyclic or periodic in nature. Now consider a simple spring-mass-damper system under harmonic excitation in stead of the real input signals (block wave actuation) that will be taken up in the next section (as the Fig.14 on page 50). Therefore, a second-order system with an input-output differential equation can obtained

$$M\ddot{y} + ky = \overline{F}\sin(wt) - F_{chamber} \qquad (2.34)$$

where $M$, $k$ are mass, spring constant, respectively. The spring is the micro-diaphragm.

The actual input driving signals can be closely approximated by sinusoidal waveforms. Any physical periodic phenomena may be represented by an infinite sum of harmonically related sinusoids, and therefore knowledge of the system frequency response to a sinusoidal input provides a basis for determining the response to a broad class of periodic inputs. Now, the core of the problems is how to define the flow resistance exerted on the micro-diaphragm.

We assume viscous liquid at volume flow rate, Q, is pumped through the central diaphragm and the narrow gap between the parallel disks (as the Fig.11) [29]. The flow rate is low, so the flow is laminar and the pressure gradient due to convective acceleration in the gap is negligible compared to the gradient due to viscous forces. We assume that the velocity profile at any cross section in the gap is the same as for fully developed flow between stationary parallel

plates. Here the flow is axisymmetric and therefore it is most convenient to take the control volume as annular ring. It is of length, $dr$, and has circumference, $2\pi r$.

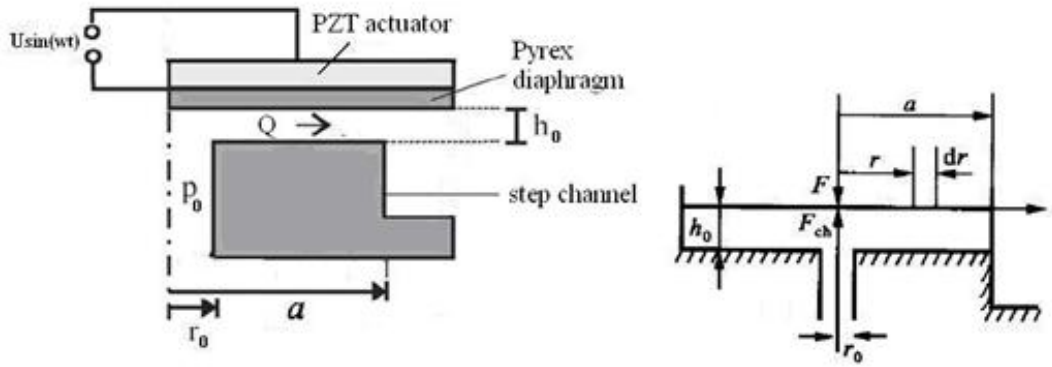


Fig. 11 A simplified model for diaphragm micropump

Therefore, the pressure gradient, $dp/dr$, as a function of radius is

$$\frac{Q}{2\pi r} = -\frac{1}{12}\left(\frac{\partial p}{\partial r}\right)h_0^3 \Longrightarrow \frac{dp}{dr} = -\frac{6\mu Q}{\pi h_0^3 r} \qquad (2.35)$$

And the flow rate Q can be approximate estimated

$$Q = \pi(a^2 - r^2)\dot{y} \qquad (2.36)$$

From (2.11), we know the solution $y(t)$ is the sum of a homogeneous component and a particular solution $y_p(t)$

$$y(t) = \sum_{i=1}^{n} C_i e^{\lambda_i t} + y_p(t) \qquad (2.37)$$

Where ***n*** is the system order (for our case ***n*** =2), $\lambda_i$ are the roots (assumed to be distinct) of the characteristic equation, and $C_i$ are n

constants to be determined from the initial conditions. The solution to the homogeneous part decays exponentially with time and is only initially significant. The particular solution is a steady state oscillation of the same frequency as the excitation and it can be assumed to be of the form, $w$ the angular frequency (rad/sec)

$$y = A_d \sin(wt - \phi), \quad \dot{y} = wA_d \cos(wt) \tag{2.38}$$

Now substitute the result (2.36) into Eq. (2.35) and integrate to find the pressure distribution

$$P = P_0 + \frac{6\mu\dot{y}}{h_0^3}\left(a^2 \ln\frac{r}{a} - \frac{1}{2}r^2 + \frac{1}{2}a^2\right), \quad (r_0 < r < a) \tag{2.39}$$

The force acted on the micro-diaphragm is given by $F_{ch} = \int_0^a p(r) 2\pi r dr$

Thus the flow resistance can be evaluated

$$F_{ch} = \pi a^2 p_0 + \frac{12\pi\mu\dot{y}}{h_0^3}\left\{a^4\left[\frac{1}{4} + \frac{1}{2}(\frac{r_0}{a})^2\right]\left[\ln(\frac{r_0}{a}) - \frac{1}{2}\right] - \frac{1}{8}(a^2 - r_0^2)^2\right\} \tag{2.40}$$

The viscous damping constant is proportion to the micro-diaphragm velocity, $wA_d \cos(wt)$; therefore we can find the damping constant.

$$C = \frac{12\pi\mu a^4}{h_0^3}\left\{\left[\frac{1}{4} + \frac{1}{2}(\frac{r_0}{a})^2\right]\left[\ln(\frac{r_0}{a}) - \frac{1}{2}\right] - \frac{1}{8a^4}(a^2 - r_0^2)^2\right\} \tag{2.41}$$

Thus, the main four parameters： the fluid viscosity $\mu$, the chamber height $h_0$, the micro-diaphragm length $a$, the geometric constants $\ln(\frac{r_0}{a})$ are necessary to determine the performance of a simplified

model for diaphragm micropump on the damping effects.

Substitute the Eq. (2.41) into (2.34) can obtain

$$M\ddot{y} + c\dot{y} + ky = \overline{F}\sin(wt) - \pi a^2 p_0 \tag{2.42}$$

Introduce the notations： $w_n^2 = \frac{k}{M}$ ， $\varsigma = \frac{c}{2\sqrt{mk}}$

We know that the magnitude of the transfer function for a forced-excited system is given by

$$A_d = |g(w)| = \frac{\overline{F} - \pi a^2 p_0}{m} \frac{1}{\sqrt{(w_n^2 - w^2)^2 + (2\varsigma w w_n)^2}} \tag{2.43}$$

To determine the frequency at which our amplitude-response curve is a maximum(which we will call the damped oscillation frequency, $w_d$)， we need only differentiate with respect to $w$ and set the result equal to zero . Thus, we obtain [30]

$$w_d = w_n\sqrt{1 - 2\varsigma^2} = w_n\sqrt{1 - \frac{c^2}{Mk}} \tag{2.44}$$

where $w_n = \sqrt{\frac{k}{M}}$ is the natural frequency of the micro-diaphragm in vacuum and $\varsigma = \frac{C}{2\sqrt{Mk}}$ is the damping factor which is drawn on to modify the natural frequency of the actuating diaphragm in vacuum. Hence, a damped frequency of the micro-diaphragm can be obtained with varying damping factor for light damping$(\varsigma \le \frac{1}{\sqrt{2}})$. From Eq. (2.44), the resonance peak occurs at a frequency less than the

undamped natural frequency $w_n$, with the shift increasing toward zero as the damping is increased. We define the difference between the damped and nature frequency as the frequency shift. In the following chapter "fabrication and test "I shall be examining the phenomena of frequency shift through experiments.

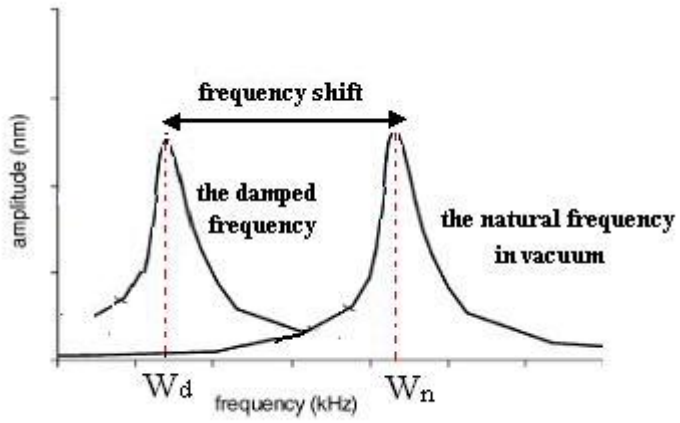


Fig. 12 The illustration of frequency shift

## 2.6 The System Dynamic for a Peristaltic Micropump

The coupled fluid–structure–electric interaction problem may be considered as a three field problem, i.e. fluid flow, structural deformation and the electric field (see Fig. 14). The effectiveness of a system is intrinsically related to its dynamic behavior. The governing equations are: Piezoelectric constitutive equation, spring-mass-damper systems and Navier–Stokes equation.

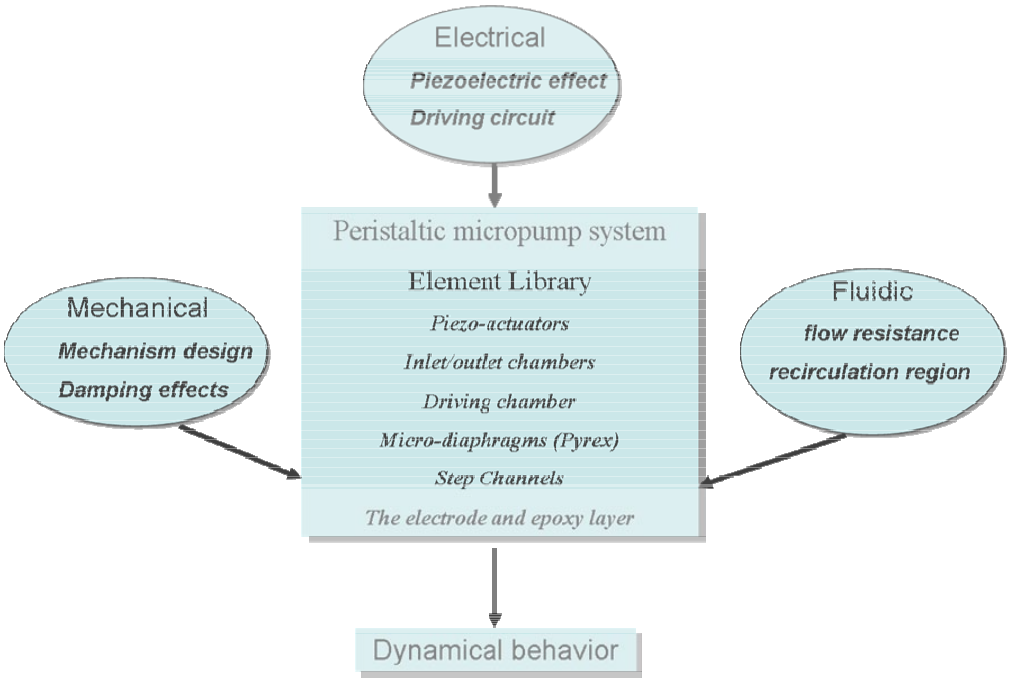


Fig. 13 The general environment for the system

## 2.6.1 Electrical Field

We introduce the phase durations for $j = 1 \ldots 6$, as defined in figure 13. The actuation sequences of a 3, 4, and 6 driving phase can refer to figure 5. The cycle duration $T$ is the sum of all $T_j$. We also introduce the relative duration of each phase $t_j = T_j / T$. The driving scheme is therefore defined by all $t_j$ and the total duration $T$. The driving frequency is defined as $f = 1/T$.

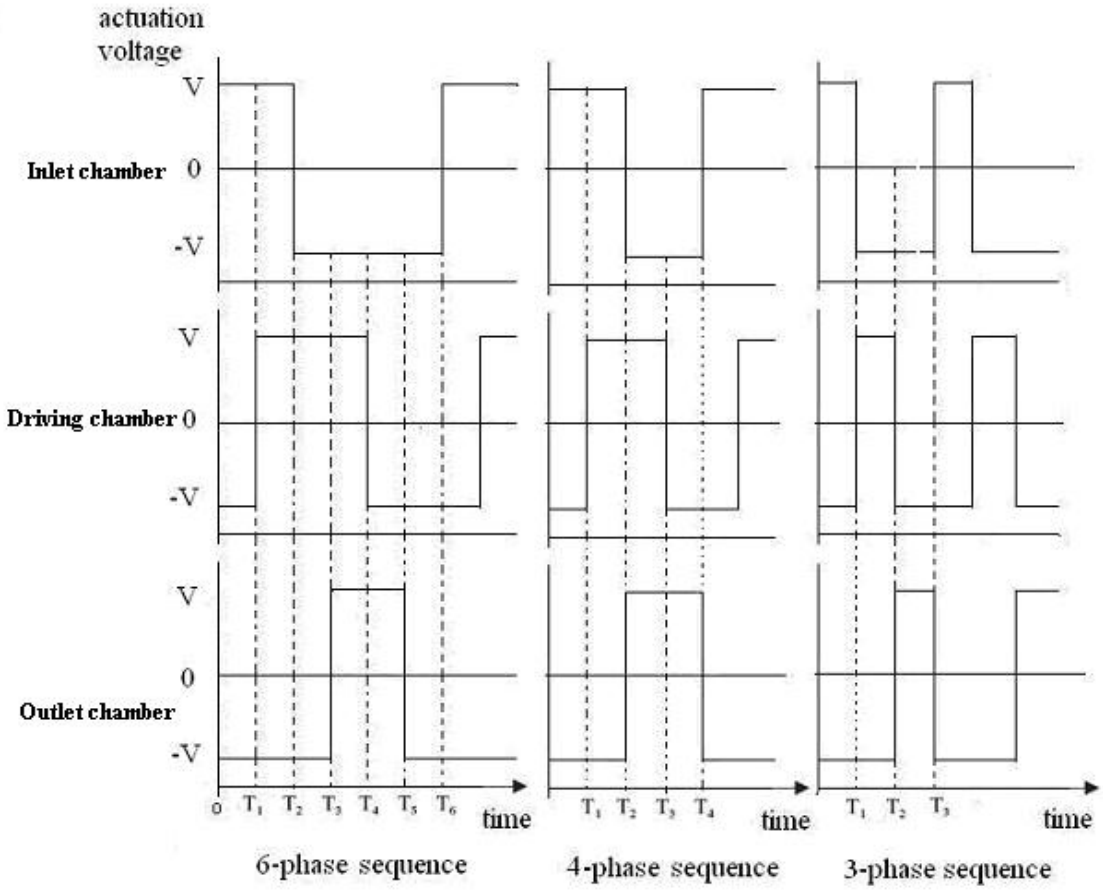


Fig. 14 Definition of the 3, 4 and6 phase durations.

By comparison with the driving signals of the valveless rectification micropump (diffuser/nozzle), we design the so called "2-phase sequence" driving signals. The three chambers have no signals phase lag. We will discuss the resonance frequency peak shift due to different phase sequence later.

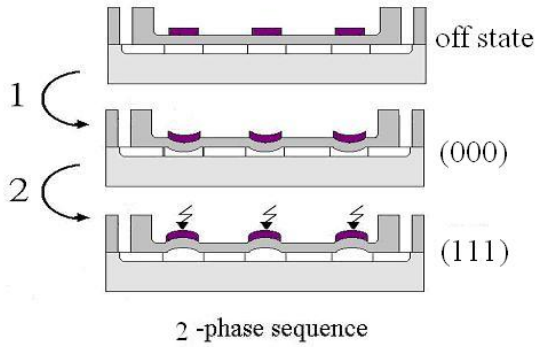


Fig. 15 Actuation sequences of a 2-phase peristaltic micropump

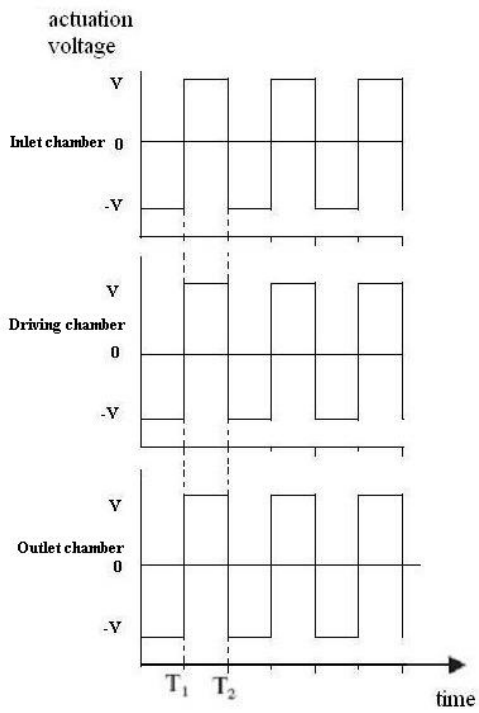


Fig. 16 Definition of the 2-phase durations.

Table 2 The comparison between cycle frequency and driving sequence

Phase Frequency ($A$ Hz)

| Driving sequence | Time step (sec) | Cycle duration (sec) | Cycle frequency (1/sec) |
|---|---|---|---|
| 2-phase | $1/A$ | $1\times 2/A$ | $A/2$ |
| 3-phase | $1/A$ | $1\times 3/A$ | $A/3$ |
| 4-phase | $1/A$ | $1\times 4/A$ | $A/4$ |
| 6-phase | $1/A$ | $1\times 6/A$ | $A/6$ |

To investigate the pump performance of micropump, the pump was actuated with the operation frequency, i.e. the phase frequency. Furthermore, the cycle frequency means the oscillation times of the micro-diaphragm through a period. Table 2 illustrates the value of cycle frequency at different driving sequence. As a example of the operation (phase) frequency 120Hz, the cycle frequency of 2, 3, 4, and 6 phase sequence are 60 , 40, 30 and 20 times respectively. It reveals the oscillation frequency of 3-phase sequence is higher than those by the 4-phase and 6-phase sequences during the same time interval. Since sinusoidal waveforms are used as the basis for representing other periodic and transient waveforms through the process of Fourier synthesis, it seems reasonable to draw an analogy between 2-phase sequence and sinusoidal waveforms for explaining the movement of micro-diaphragm. Consequently, the cycle frequency factor $\alpha$ presented in Table 3 is drawn on to modify 3, 4, and 6 phase sequence.

Table 3 The cycle frequency factor

| Driving sequence | The cycle frequency factor |
|---|---|
| 2-phase | $\frac{A}{2} = W$ |
| 3-phase | $\frac{A}{3} \times \frac{2}{3} \div \frac{A}{2} = 0.444\ W$ |
| 4-phase | $\frac{A}{4} \times \frac{1}{2} \div \frac{A}{2} = 0.25\ W$ |
| 6-phase | $\frac{A}{6} \times \frac{1}{2} \div \frac{A}{2} = 0.167\ W$ |

Therefore, Using Eq. (2.38), (2.41), (2.44) and Table.3, we should consider the cycle frequency factor $\alpha$ to correct Eq. (2.41) into (2.45)

$$c = \frac{\alpha \cdot 12\pi\mu a^4}{h_0^3}\left\{\left[\frac{1}{4}+\frac{1}{2}\left(\frac{r_0}{a}\right)^2\right]\left[\ln\left(\frac{r_0}{a}\right)-\frac{1}{2}\right]-\frac{1}{8a^4}(a^2-r_0^2)^2\right\} \qquad (2.45)$$

Where $\alpha_{3-phase} = 0.444$, $\alpha_{4-phase} = 0.25$ and $\alpha_{6-phase} = 0.167$

## 2.6.2 Mechanical Field

In the section, the geometrical dimensions of the actuator and the diaphragm and the chamber height are design which can produce more displacement without complicated fabrication, leading to a higher expansion/compression ratio.

Alternating voltage causes the PZT component to expand and contract along the horizontal direction. This induces a bending stress on the diaphragm, which in turn pumps the fluid through the

chamber. From the simulations below, we turn up the interesting facts that the maximum stresses occur near the edge of the diaphragm ($0.01 < r < 0.012\ m$) where the largest bending moments exist (Fig. 19 and 20).

To assure pump reliability for high cycle fatigue, it is, therefore, necessary to design this pump so that the maximum stress level is kept lower than the stress endurance limit of the diaphragm material. This requirement is vital for many types of micro devices considering the role micro pumps play in sustaining the reliability of MEMS for biomedical applications, such as lab-on-a-chip devices. Consequently, we can take the concept of reliability analysis (lifetime, operating time and electric load of a piezoelectric actuator micropump) into consideration further in the future.

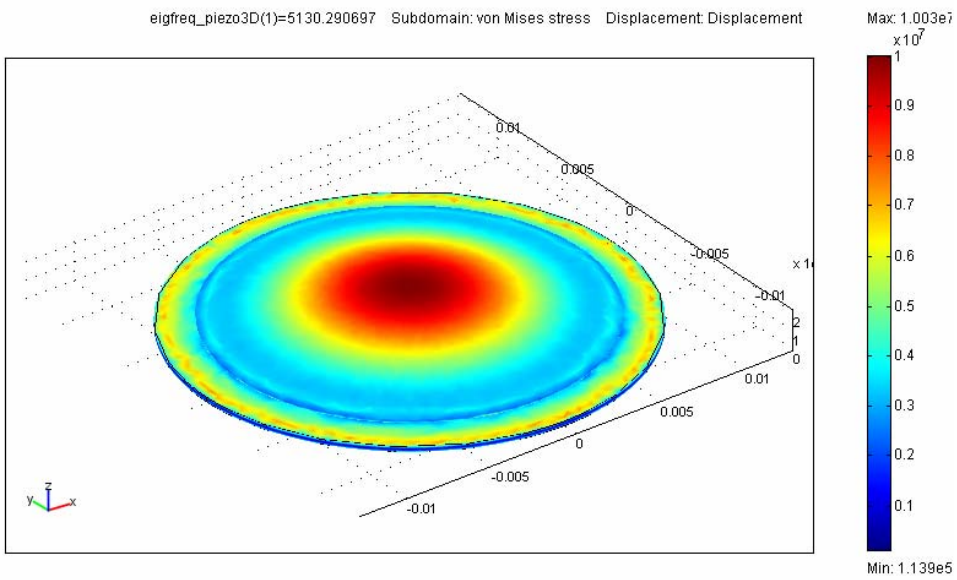


Fig. 17 A top view of the stresses obtained from FEM analysis in the 1st mode frequency

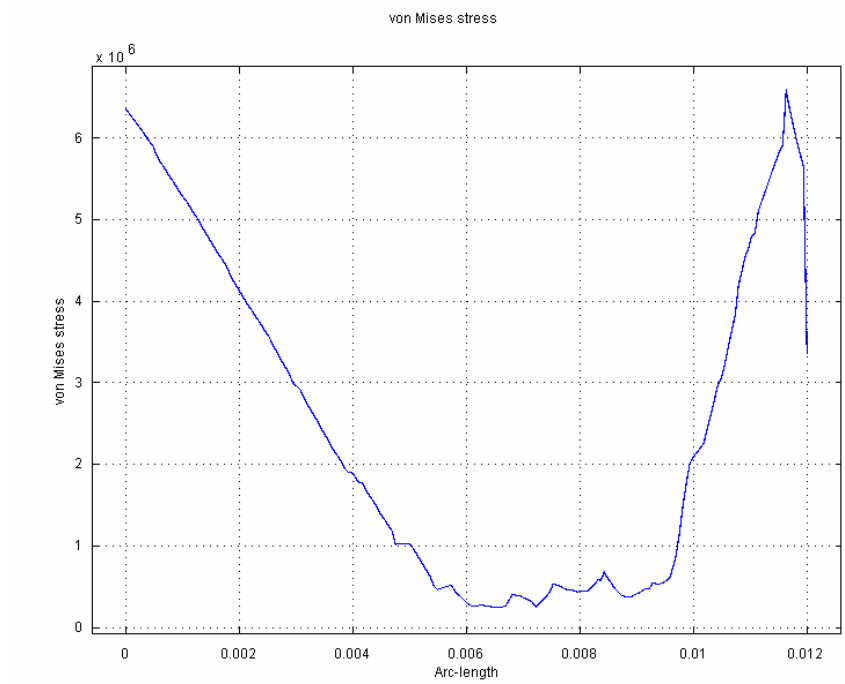


Fig. 18 The stress distributed at different position in the 1st mode

### 2.6.3 Governing Equations

A piezoelectric patch is utilized as the actuator. PZT-5H, a special type of piezoelectric, is used in the simulation. Properties of PZT-5H are given in table1. The coupled electro-mechanical constitutive equation for the actuator is

$$\sigma_{ij} = C^{E}_{ijkl}\varepsilon_{kl} - e_{ijk}E_k \tag{2.46}$$

where $\varepsilon_{kl}$ is the mechanical strain tensor, $\sigma_{ij}$ is the mechanical stress tensor, $E_k$ is the electric field vector, $e_{ijk}$ is the piezoelectric constant tensor; $C^{E}_{ijkl}$ is the elastic stiffness constant tensor at constant electric field and it is a 6 × 6 symmetric tensor.

Table 4 Properties of PZT-5H [31]

| | | | |
|---|---|---|---|
| Relative Dielectric Constant (@ 1 KHz) | $K^T_3$ | 3800 | |
| Piezoelectric Strain Coefficient | $d_{33}$ | $650 \times 10^{-12}$ | meters/Volt |
| | $d_{31}$ | $-320 \times 10^{-12}$ | meters/Volt |
| Piezoelectric Voltage Coefficient | $g_{33}$ | $19.0 \times 10^{-3}$ | Volt meters/Newton |
| | $g_{31}$ | $-9.5 \times 10^{-3}$ | Volt meters/Newton |
| Coupling Coefficient | $k_{33}$ | 0.75 | |
| | $k_{31}$ | | |
| Polarization Field | Ep | $1.5 \times 10^6$ | Volts/meter |
| Initial Depolarization Field | Ec | $3.0 \times 10^5$ | Volts/meter |
| **MECHANICAL** | | | |
| Density | | 7800 | $Kg/meter^3$ |
| Mechanical Q | | 30 | |
| Elastic Modulus | $Y^E_3$ | $5.0 \times 10^{10}$ | $Newtons/meter^2$ |
| | $Y^E_1$ | $6.2 \times 10^{10}$ | $Newtons/meter^2$ |
| Poisson's Ratio | V | ~.31 | |
| **THERMAL** | | | |
| Thermal Expansion Coefficient | | $\sim 3 \times 10^{-6}$ | meters/meter °C |
| Curie Temperature | | 250 | °C |

The Pyrex diaphragm in the peristaltic micropump is integrated with surrounding walls; therefore, it can be considered as a clamped plate as the Figure 19. The governing equation of forced vibration of a thin clamped plate is

$$D\nabla^4 W + \rho_{Pyrex} h \frac{\partial^2 W}{\partial t^2} = f_e - P \qquad (2.47)$$

where

$$D = \frac{Eh^3}{12(1-\nu^2)} \qquad (2.48)$$

and $f_e$ is the periodic actuating force, which can be solved from equation (2.46), $E$ is the elastic modulus of the Pyrex diaphragm, $\lambda$ is Poisson's ratio of the Pyrex diaphragm, $\rho_{Pyrex}$ is the density of the Pyrex diaphragm, $h$ is the thickness of the Pyrex diaphragm, and $P$ is the dynamic pressure exerted on the diaphragm by the liquid. To solve equation (2.47), $P$ should be solved from the Nervier–Stokes equations at every time step. Since we assume the diaphragm to be a clamped plate, displacements, curvatures and velocities of the clamped plate at edges should be zero. Therefore, the boundary conditions for a clamped plate can be written mathematically as

$$W = 0 \qquad x, y \in \partial\Omega \text{ (at edge)} \qquad (2.49)$$

$$\frac{\partial^2 W}{\partial x^2} = \frac{\partial^2 W}{\partial y^2} = 0 \qquad x, y \in \partial\Omega \qquad (2.50)$$

$$\frac{\partial W}{\partial t} = 0 \qquad x, y \in \partial\Omega. \qquad (2.51)$$

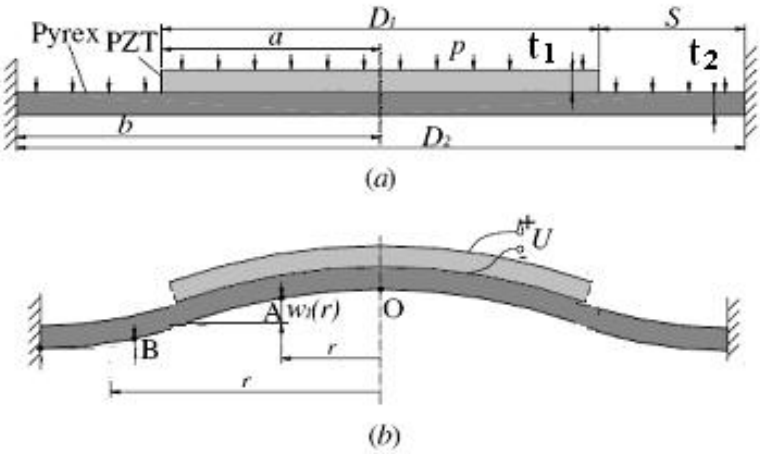


Fig. 19 **a.** Schematic of the cross section of a piezo-Pyrex-diaphragm bi-layer **b.** Deflection of the pump diaphragm $D_1$: diameter of PZT; $D_2$: diameter of Pyrex; $S$: distance between Pyrex and PZT edges; diaphragm thickness $t_1$ =191μm and $t_2$ = 150 μm

Properties of the fluid used in this simulation are listed in table 5. Since the characteristic length of the micropump is of the order of $10^{-6}$ and the Reynolds number is very low, the flow can be considered as an incompressible laminar flow, which can be described using the Navier–Stokes equations (2.52) and the mass continuity equation (2.53)

$$\rho_L \mathrm{D}\vec{V}/\mathrm{D}t = \rho_L \vec{g} + \mu \nabla^2 \vec{V} - \nabla P \qquad (2.52)$$

$$\frac{\partial \rho_L}{\partial t} + (\vec{V} \cdot \nabla)\rho_L = 0. \tag{2.53}$$

Table 5 Fluid properties

| Property | Density $\rho_L$ | Dynamic viscosity $\mu$ |
|---|---|---|
| Unit | kg m$^{-3}$ | $\times 10^{-3}$ kg m$^{-1}$ s$^{-1}$ |
| Value | 1000 | 1.4 |

In this study, the commercial software CFD-ACE+ is used to solve the piezo-diaphragm-fluid coupling for multidisciplinary analysis. The solution algorithm for full coupling is shown in Fig.21.The broad approach is conventional in that the fluid and the structure are solved sequentially. The model considered is shown in Fig. 22. with three layers: a square PZT stack which is easier to manufacture than a corresponding circular multi-layer stack, silicon diaphragm and chamber with two outlets. In the design of the model, the silicon diaphragm is fully covered by a PZT layer and the chamber is fully covered by the PZT–silicon diaphragm bi-layer. Fig. 23.(a)(b) indicate the dynamic analysis result of the vertical displacement and pressure of a point centered on diaphragm-fluid interface respectively. The deflections at different actuating frequencies are presented in Table 6.

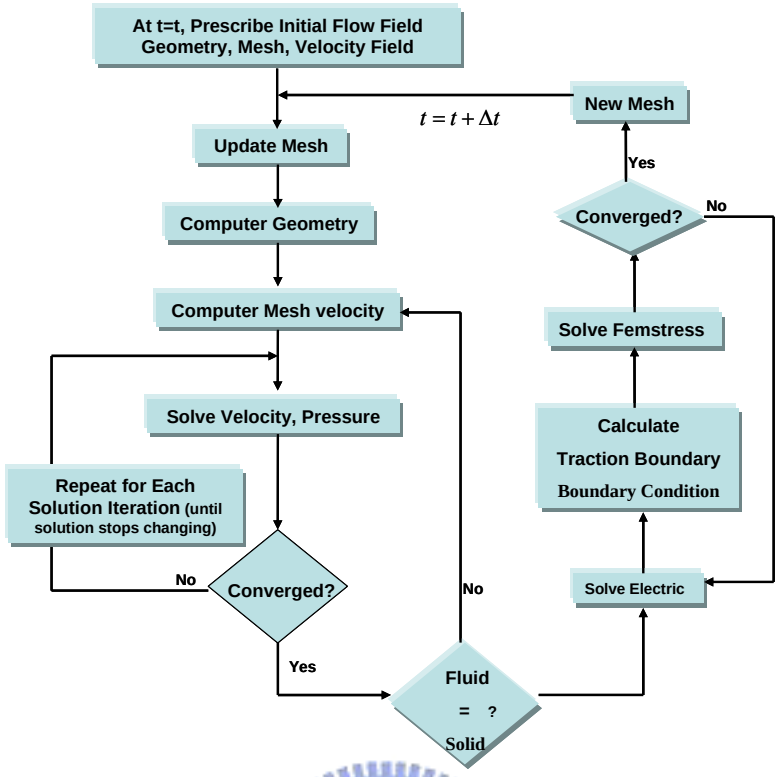


Fig. 20 The solution algorithm for piezo-diaphragm-fluid coupled solver

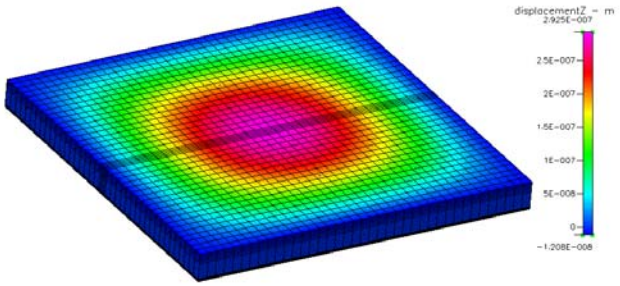


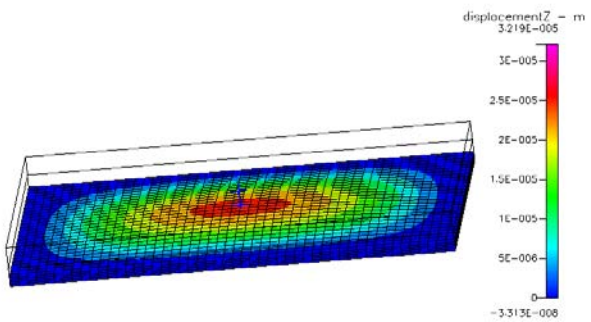

Fig. 21 The three layers model under 100Hz sinusoidal excitation (water, 100V). Grids at the center area of each layer are denser.

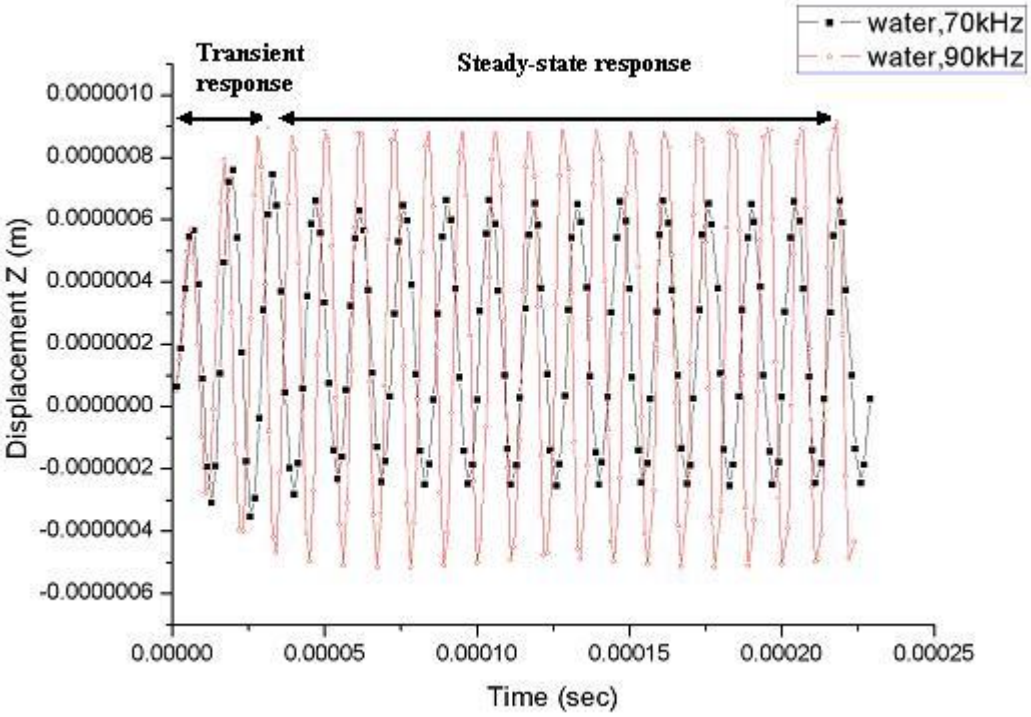


(a)

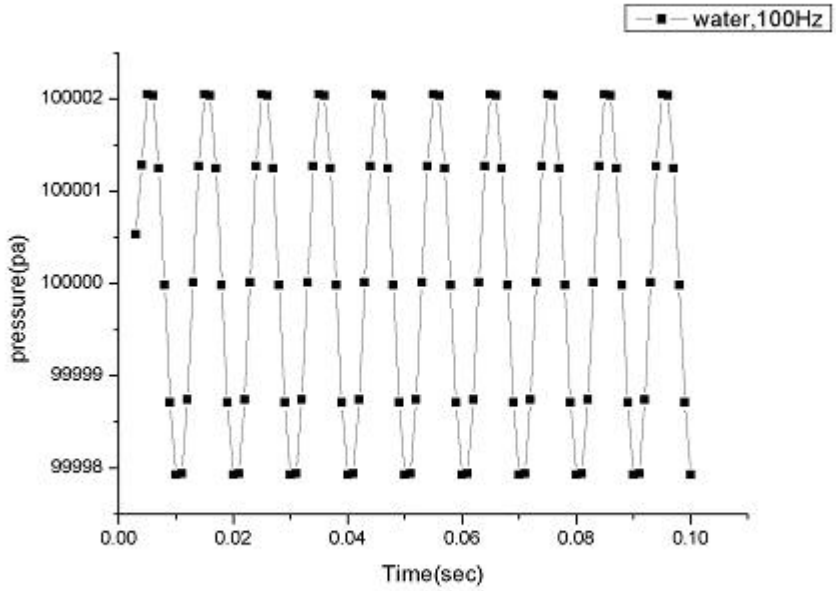


(b)

Fig. 22 (a) Transient behavior of displacement

(b) Transient behavior of chamber pressure

Fig. 23 shows the time history of the vertical displacement of a point on the top of the PZT piezoelectric component. This displacement is directly related to the vertical motion corresponding to the 1st mode. The effect of resonance becomes apparent under the nature frequency. In the transient analysis, a dynamic maximum displacement of 0.9μ*m* is reached after 3 cycles a 90k Hz.

Table 1 The deflections at different actuating frequencies (water)

| Frequency(Hz) | Max. deflection(μm) | Frequency(Hz) | Max. deflection(μm) |
|---|---|---|---|
| 50 | 0.354 | 70000 | 0.722 |
| 100 | 0.354 | 80000 | 0.759 |
| 500 | 0.354 | 90000 | 0.842 |
| 1000 | 0.402 | 100000 | 0.884 |
| 5000 | 0.508 | 110000 | 0.821 |

a photograph (as Fig.24) of the finished micropump with the size of 20 mm by 20 mm. diaphragm thickness $t_1$ =191μm and $t_2$ = 300 μm

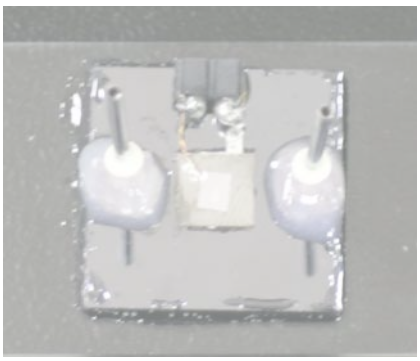

Fig. 23 The photo of the finished diffuser/nozzle micropump

Fem Solver: Eigen Values and frequencies

| Mode# | Eigen Value | Frequency |
|---|---|---|
| 1 | 5.896794e+009 | 1.222160e+004 |
| 2 | 3.192904e+010 | 2.843892e+004 |
| 3 | 3.283603e+010 | 2.884001e+004 |
| 4 | 8.692605e+010 | 4.692401e+004 |
| 5 | 1.386701e+011 | 5.926681e+004 |

The disagreement of resonance frequency between the simulation and experiment indicates the actual system included the inlet and outlet tubes, and an electric connector fixed on the micro-diaphragm device by epoxy.

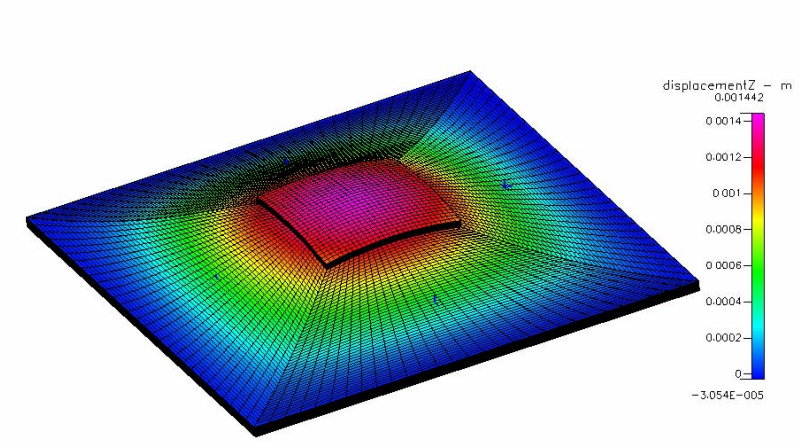

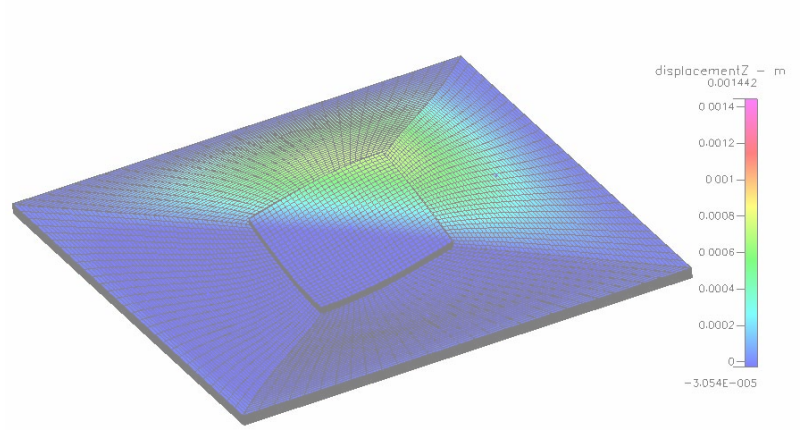
displacementZ – m
0.001442
0.0014
0.0012
0.001
0.0008
0.0006
0.0004
0.0002
0
-3.054E-005

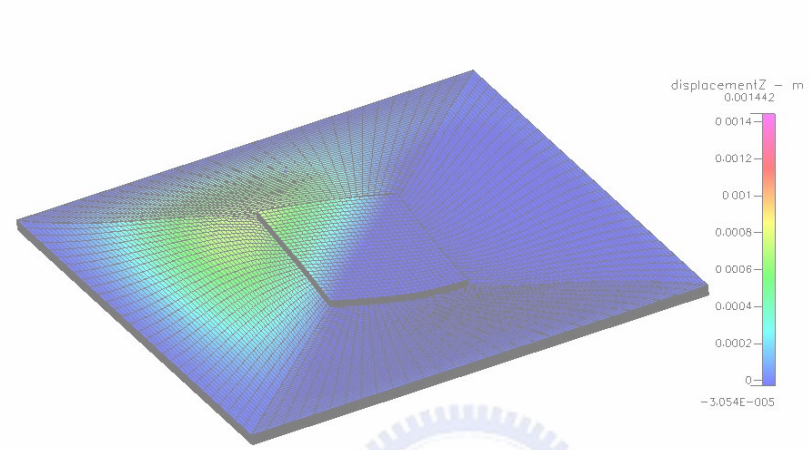
displacementZ – m
0.001442
0.0014
0.0012
0.001
0.0008
0.0006
0.0004
0.0002
0
-3.054E-005

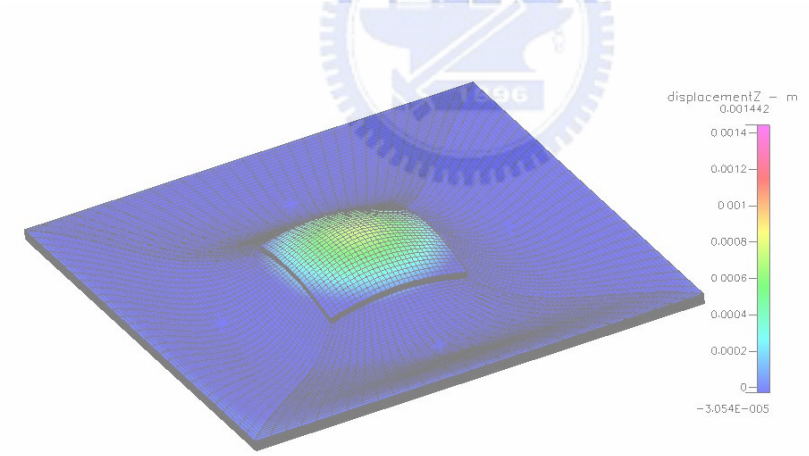
displacementZ – m
0.001442
0.0014
0.0012
0.001
0.0008
0.0006
0.0004
0.0002
0
-3.054E-005

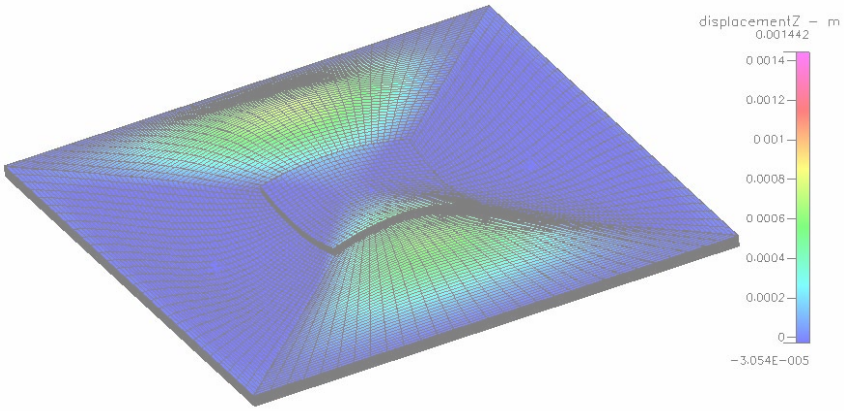
displacementZ – m
0.001442
0.0014
0.0012
0.001
0.0008
0.0006
0.0004
0.0002
0
-3.054E-005

Fig. 24 The modal shape analysis for PZT and Si diaphragm bi-layer

### 2.6.4 Flow Field

Unlike solids, fluids don't stay where they are put . When subjected to shear forces, they deform with limit, and because of their viscosity, this deformation is inherently dissipative and irreversible. However, fluids do have elastic properties when subjected to normal forces (pressure). And they have inertial. Thus, just like an elastic medium, fluids can propagate sound waves. Our goal is to introduce basic fluidic behaviors, and focus on the phenomena that are important in the chambers of the peristaltic micropumps by simulation.

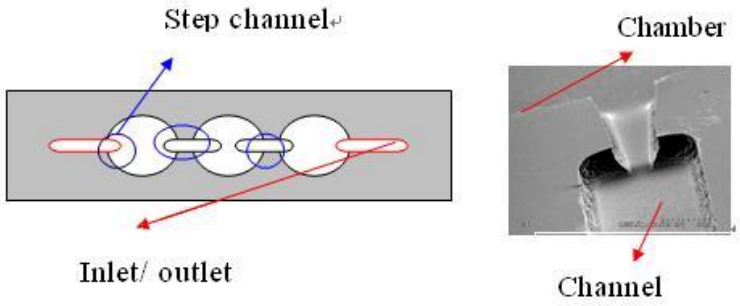


(a)




(b)

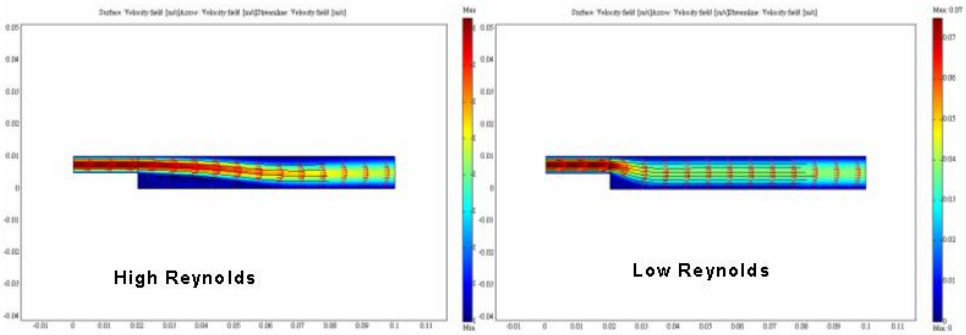


(c)

Fig. 25 (a) Schematic of the peristaltic micropump (b) SEM photo of the step channel (c) Recirculation region

**Case of rectangular channel**

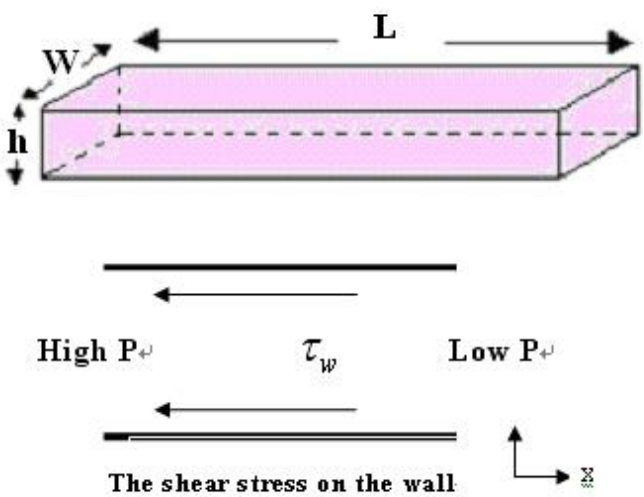


Fig. 26 Schematic representation of the rectangular channel

For many devices the flow-pressure characteristic can be described using a simple analytical formula well known from macroscopic fluid mechanics as for microchannel or nozzle diffuser. This is the application of the Navier-Stokes equations. We now consider a pressure-driven flow between stationary parallel plates.

Assumption：

1. The flow is horizontal, so there is no contribution from gravity.
2. The velocity in the x-direction is only a function of y.
3. a uniform pressure gradient in the x-direction, namely

$$\frac{dp}{dx} = -k \text{ (constant)}$$

With these assumptions, the Navier-Stokes equation becomes

$$\frac{\partial^2 U_x}{\partial y^2} = -\frac{k}{\mu}$$

This equation has a quadratic-polynomial solution. With the no-slip boundary condition, the solution becomes

$$U_x = \frac{1}{2\mu}\left[y(h-y)k\right]$$

The volumetric flow rate Q

$$Q = W\int_0^h U_x dy = \frac{Wh^3}{12\mu}K$$

In the case, the pressure gradient must be expressed in terms of the pressure drop between the ends $\Delta P$, spaced by a length L.

$$K = \frac{\Delta P}{L}$$

The relation between flow and pressure drop is then

$$\Delta P = \frac{12\mu L}{Wh^3}Q$$

The lumped element model for a Poiseuille flow path is

$$R_{pois} = \frac{12\mu L}{Wh^3} \qquad (2.54)$$

This is a particular useful equation for calculating the pressure drop through a long channel.

# CHAPTER 3
# FABRICATION AND TEST

## 3.1 Design and Fabrication of a Peristaltic Micropump

The micropump consists of three parts: silicon, Pyrex glass, and a commercially available bulk PZT chip (Piezo Systems, Inc., T107-H4E-602). The silicon etching process was used to create pump chambers and channels. The Pyrex glass etching another process was used to create pump diaphragm. In the glass part: In order to create deep etching glass, it was coated with polymer and then pattern it. Second, we used a 49% HF etching glass. It was achieved glass diaphragm of 150 μm thickness. Finally, the glass was removed polymer and then drilled through the glass by the diamond bit. At the silicon part: a 500-μm-thick of a (100) oriented silicon substrate. It process prior to sputter aluminium of 2000A, then silicon was used photorisists and wet etching that it is patterned channel. The channel was formed by ICP process. This process must do again, because we need to pattern chamber. The depth of the chambers and channels are 30 μm and 200 μm, respectively. Pyrex glass was stacked on the patterned silicon substrate by anodic bonding. The anodic bonding was performed at 475 $^{o}$C and 1000 V. A piece of 12 mm square bulk PZT with the thickness of 191 μm was glued and contacted on the membrane with silver epoxy. The cross view of the pump with dimension are give in Fig. 1. The inlet and outlet tubing, and the electric connector were

fixed on the device using epoxy glue.

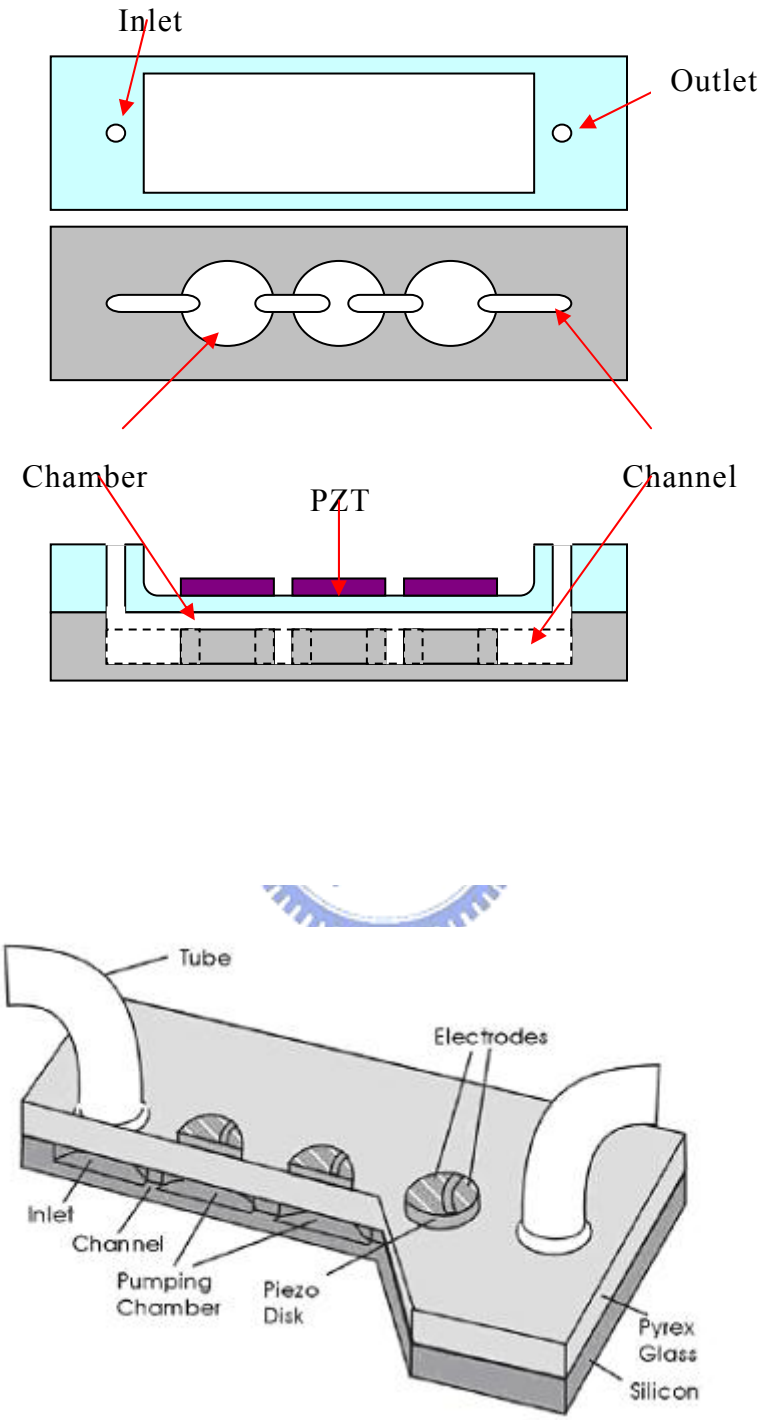


Fig. 27 Schematic of peristaltic micropumps

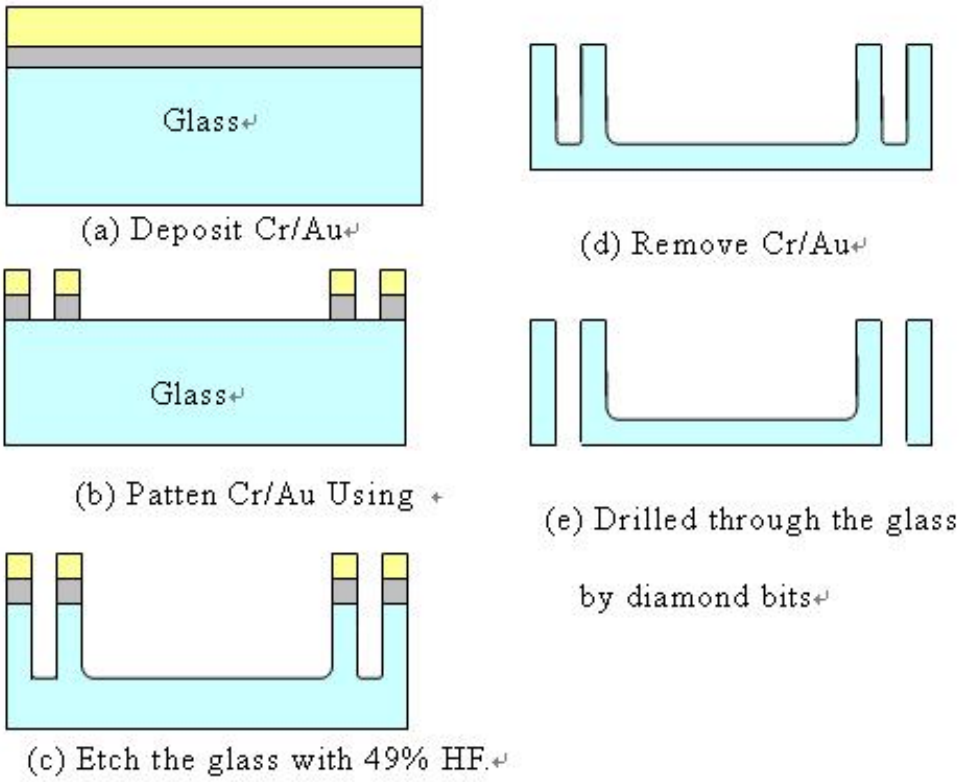


Fig. 28 Glass etching process.

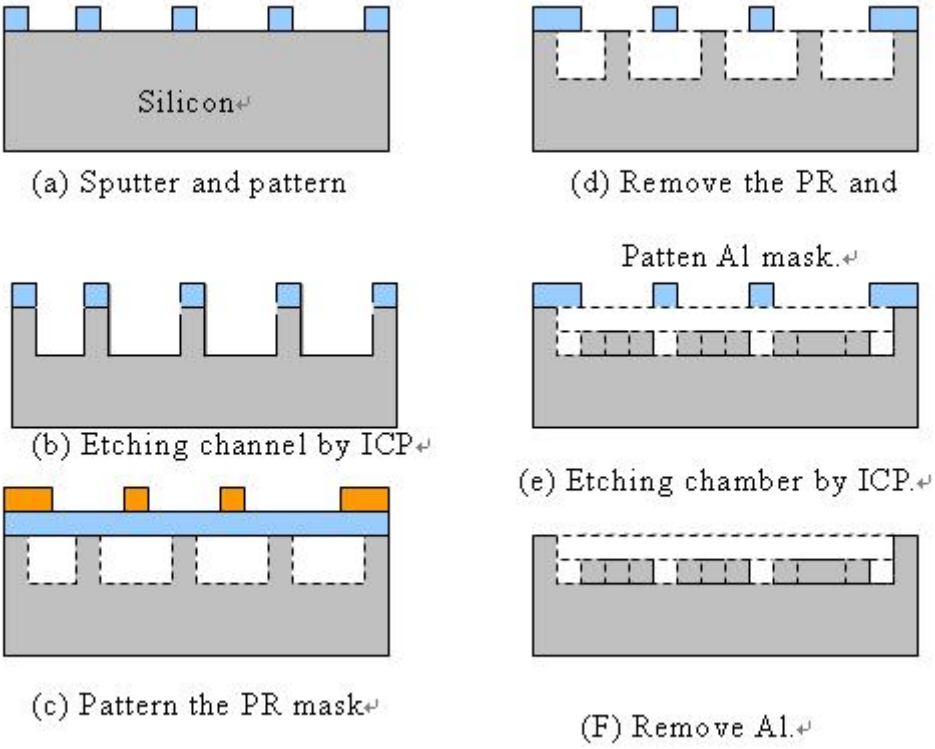

Fig. 29 Silicon etching process.

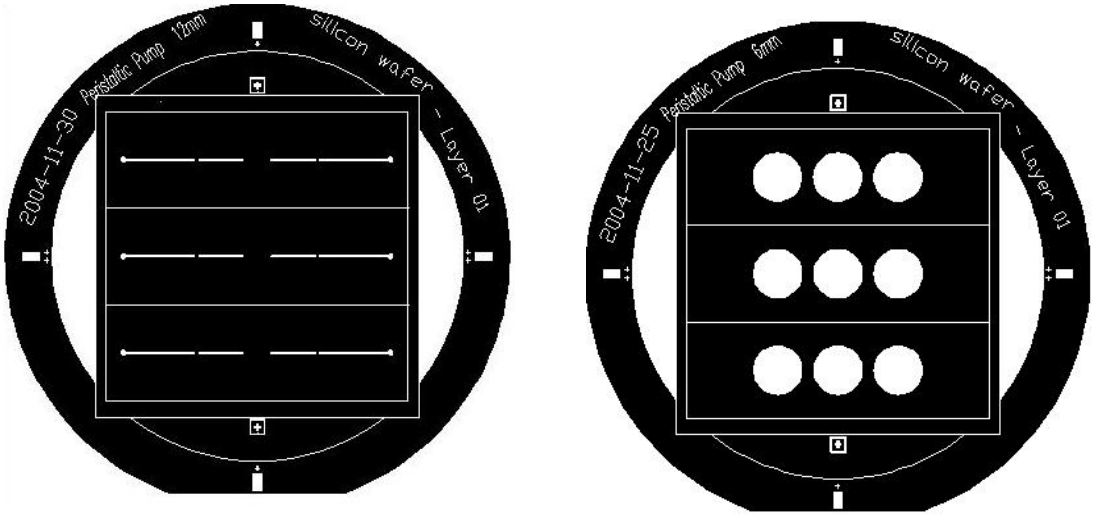


Fig. 30 The photomask of channel and chamber

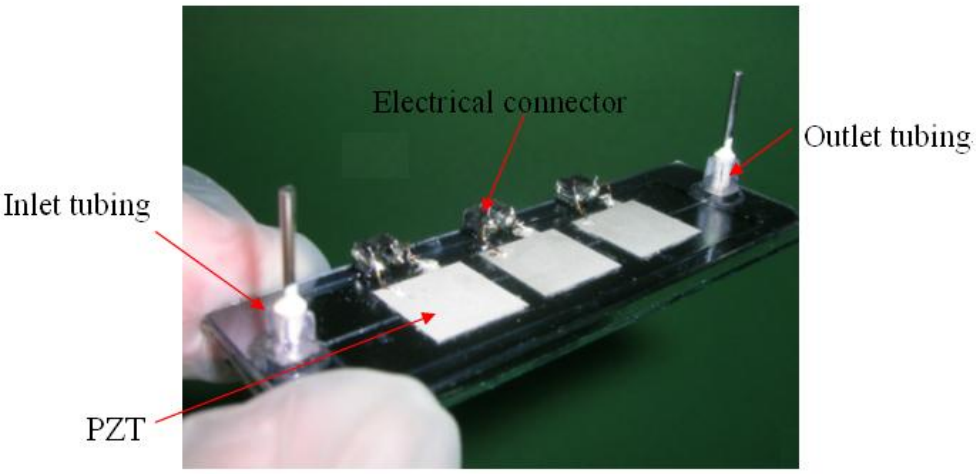


Fig. 31 The complete peristaltic micropump

## 3.2 Experimental Setup

The experimental setup is schematically shown in Fig. 32. The function generator, power amplifier (Piezotronics, PCB790) and digital oscilloscope, microbalance (Sartirius, BL 120S) and fiber-optical measurement system (MTI Instruments, MTI 2000) were used to carry out the pump performance tests. The pump was driven by an amplified step-function signal and a driver circuit to operate phase of PZT. The flow rate of the pump was obtained by the balance and timer. In order to find the displacement membrane of the pump, the frequency response test was performed. The displacement response of the pump was measured by the fiber-optic probe in terms of the peak displacement of the center of the driving piezoelectric actuator, as a function of frequency at a driving voltage, while the pumping system was filled with fluids. Two different kinds of fluids were used: DI water and whole blood. The whole blood was provided by the blood bank.

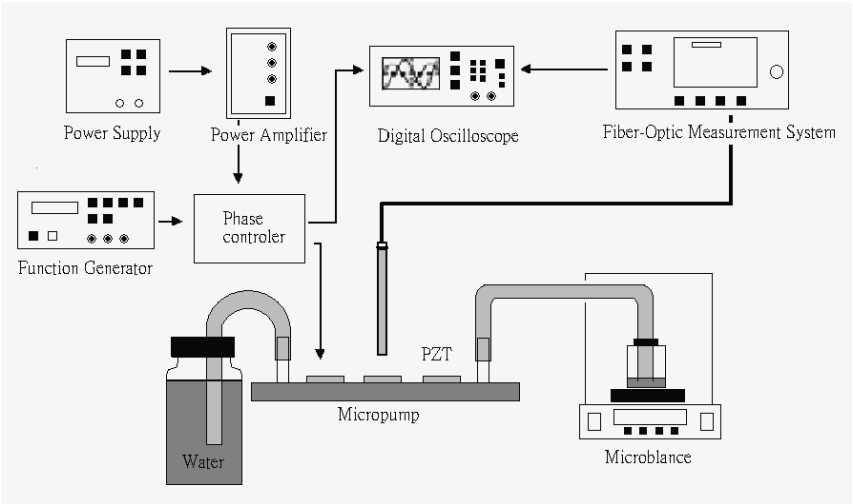

Fig. 32 The schematic of the experimental setup

## 3.3 Experiments and Results

To evaluate the pump performance, the pump was excited in the 3-, 4- and 6-phase peristaltic motions, and actuated with the step-function signals with varied phase frequencies created by the phase controller. What fascinates me about output performance is the frequency domain. Two 0.04 inch ID tubes were connected to the inlet and outlet of the peristaltic micropump.The outlet tube was placed into a reservoir on a scale. The pumping rates were calculated over a period of time from the weight of deionized water (DI water) or blood, measured by the scale. The maximum displacement of the moving diaphragm with DI water was measured by fiber-optical measurement system (MTI Instruments, MTI 2000).The fiber-optical measurement system served as a displacement sensor, monitoring the dynamic performance of the pump. The signals from the fiber-optical measurement system were recorded using a digital oscilloscope. Experimental results indicate that bidirectional flow could be achieved by reversing the actuation sequence.

# The Damping Effects on Pump Diaphragm

## A. The Phase sequence and frequency shift

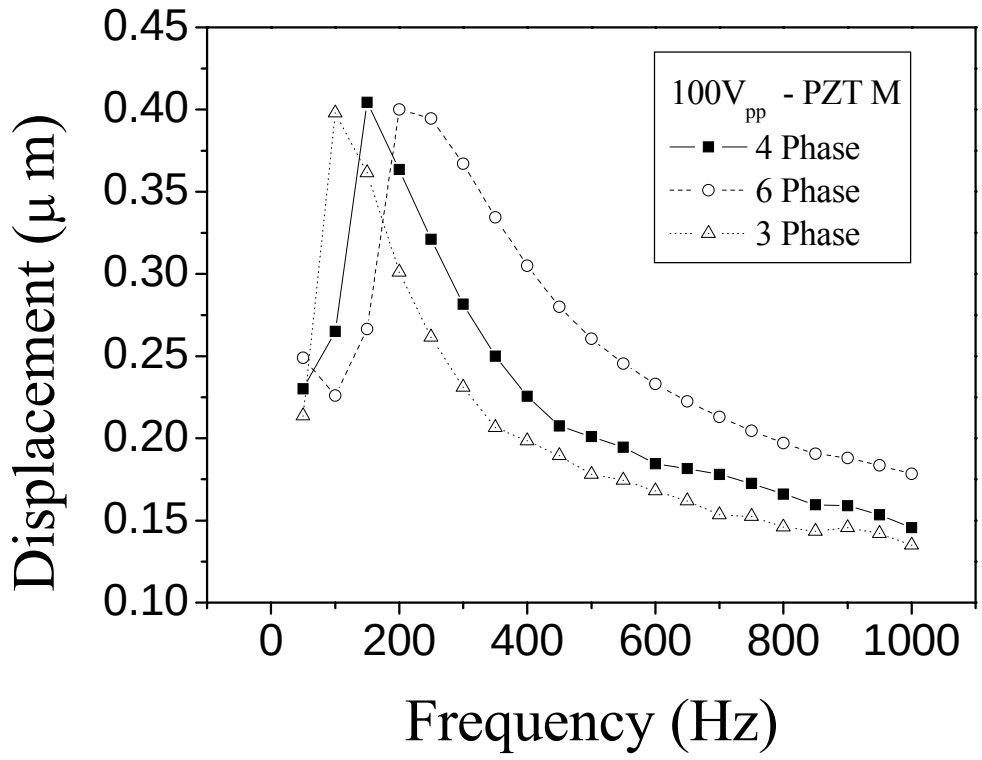


Fig. 33 Displacement of the middle moving diaphragm as a function of phase frequency at 100 $V_{pp}$(4P16)

Figure 34 shows the displacement of the middle moving diaphragm as a function of phase frequency at 100 Vpp for the 3-, 4- and 6-phase sequences. The figure indicates that different actuation sequences resulted in different resonant frequencies of the diaphragm. Using Eq. (2.44), (2.45), we can make sense of the reason why the resonant frequency shift in 3-phase sequence has a stronger tendency compared to the other two driving sequences. The

experimental displacement frequency-response curves at different phase motion (as shown in Fig. 34.) have the comparable results with the presented theoretic analysis. The resonant frequencies of the diaphragm for the 3-, 4- and 6-phase sequences were 100Hz, 150Hz and 200Hz, respectively. The maximum displacement of the diaphragm for the 3-, 4- and 6-phase actuation sequences was 3.7 $\mu m$, 4.0 $\mu m$ and 3.8 $\mu m$ (peak-to-peak), respectively.

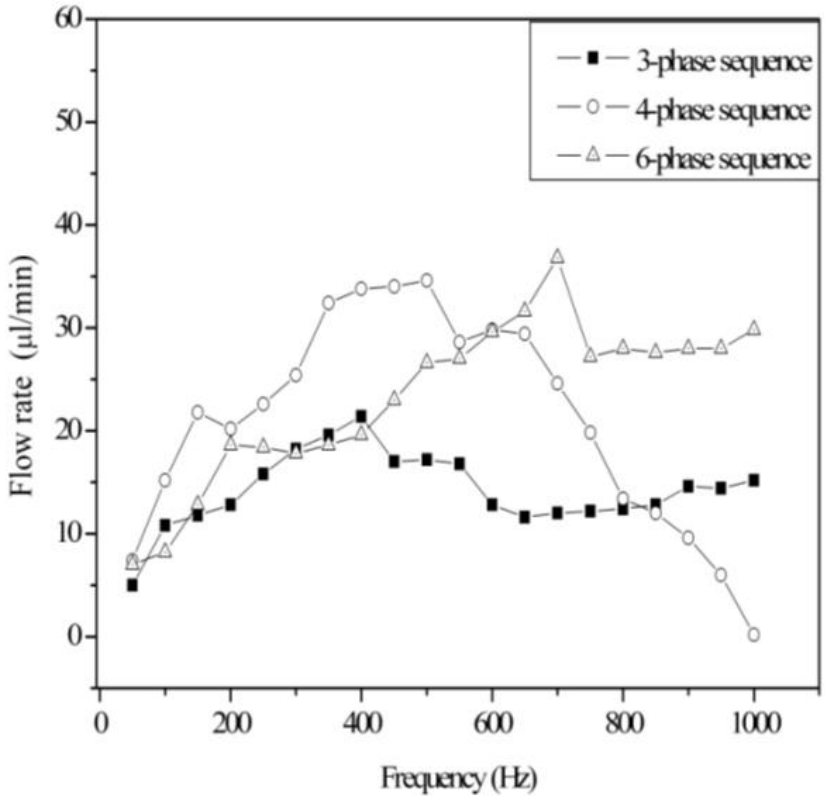


Fig. 34 Flow rate *vs.* phase frequency at 100 $V_{pp}$

Figure 35 illustrates the flow rates of the micropump at an applied voltage of 100Vpp with a phase frequency range of 50–1000Hz for the 3-, 4- and 6-phase peristaltic motions. The maximum flow rates of the 3-, 4- and 6-phase sequences occurred at

400Hz, 500Hz and 700Hz, and were 21.4μl/min, 34.6μl/min and 36.8μl/min, respectively. The same observation compared with Fig.34 applies to flow rate frequency-response curves. The frequency of resonance peak: 6-phase >4-phase >3-phase. According to Fig. 35, the flow rates peaked at a certain frequency and fell at higher frequencies for all actuation sequences. The experimental results clearly indicate that the pumping rates rose with increasing frequency at lower frequencies. The moving diaphragm was not fast enough to keep up with the actuation signal at higher frequencies, so the actuation magnitude decreased, thus reducing the pumping performance.

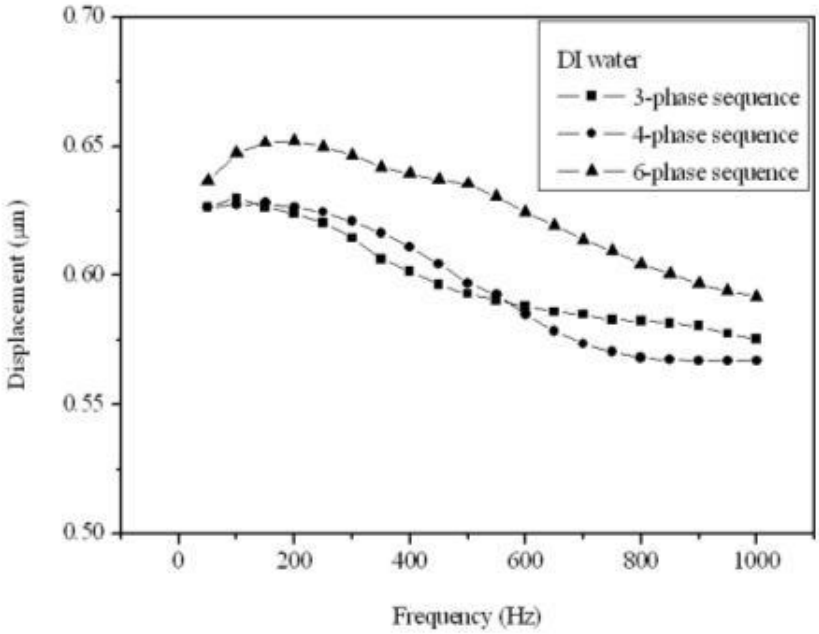


Fig. 35 Displacement of the middle moving diaphragm as a function of phase frequency at 100 $V_{pp}$ (4P20)

3 Phase-100 Hz；4 Phase-150 Hz；6 Phase-200Hz

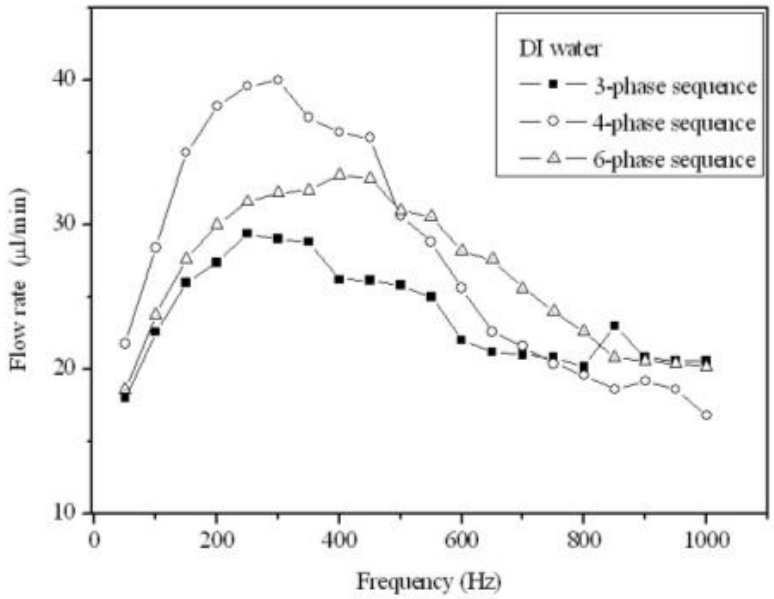


Fig. 36 Flow rate *vs.* phase frequency at 100 $V_{pp}$ (4P20)

3 Phase-250 Hz；4 Phase-300 Hz；6 Phase-400Hz

3 Phase-29.4 μl/min；4 Phase-40 μl/min；6 Phase- 33.4 μl/min

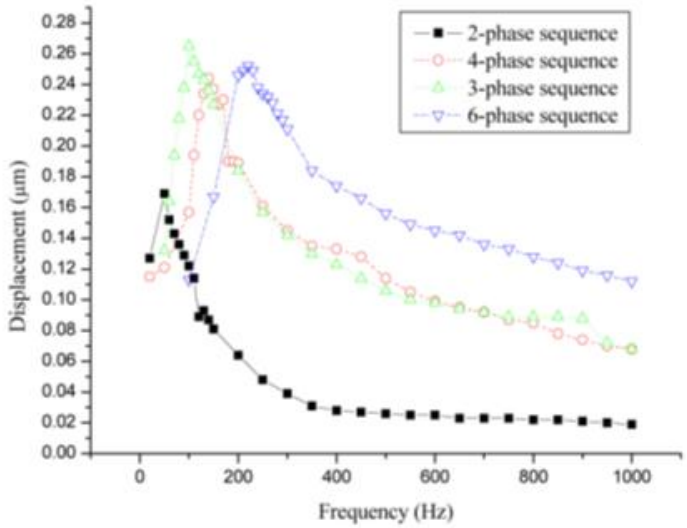

Fig. 37 The displacement frequency of 2-phase sequence

$$c = \frac{\alpha \cdot 12\pi\mu a^4}{h_0^3}\left\{\left[\frac{1}{4}+\frac{1}{2}(\frac{r_0}{a})^2\right]\left[\ln(\frac{r_0}{a})-\frac{1}{2}\right]-\frac{1}{8a^4}(a^2-r_0^2)^2\right\}$$

Where $\alpha_{3-phase} = 0.444$ , $\alpha_{4-phase} = 0.25$ and $\alpha_{6-phase} = 0.167$

$$w_d = w_n\sqrt{1-2\varsigma^2} = w_n\sqrt{1-\frac{C^2}{Mk}}$$

The frequency of resonance peak: **6-phase >4-phase >3-phase>2-phase**

## B. The working fluids and frequency shift

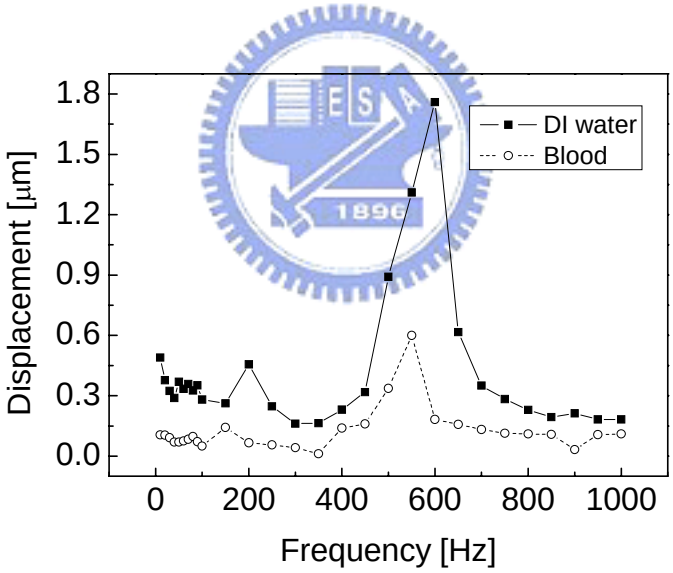


Fig. 38 The displacement of membrane versus the driving frequency at 100 V (4P10)

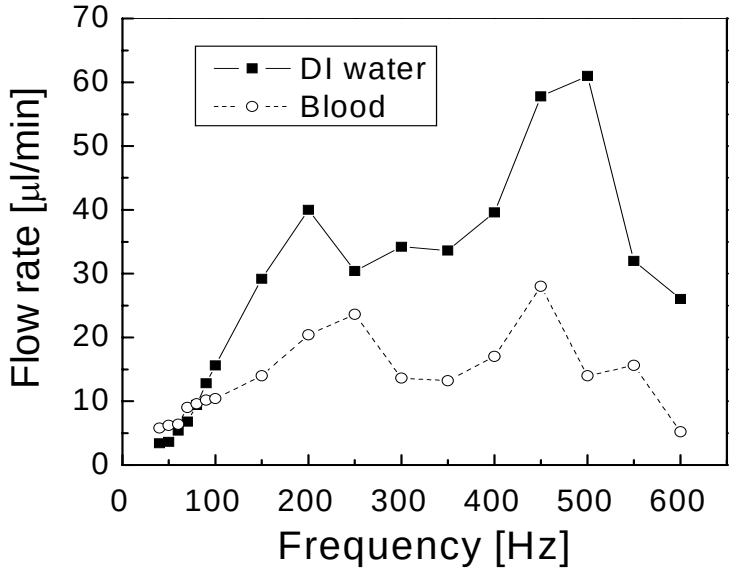


Fig. 39 The Flow rate of pumping versus the driving frequency at 100 V (4P10)

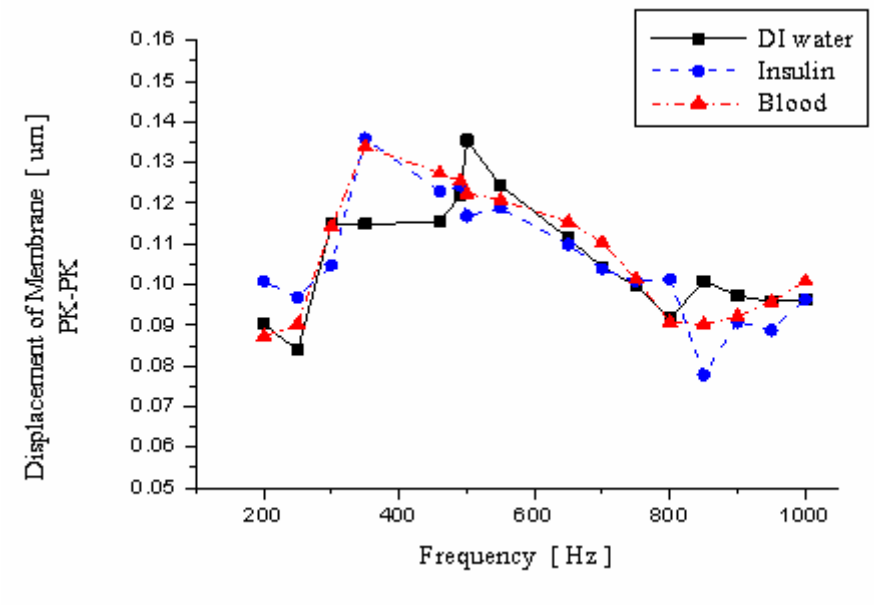


Fig. 40 The displacement of diaphragm versus the driving frequency for different working fluids.

Three kinds of working fluids were tested by diffuser/nozzle micropump: water, insulin and blood. Fig. 40 shows the displacement of the membrane for DI water, insulin and blood at the driving voltage of 10 V and frequency varied from 200 Hz to 1 KHz. The resonance frequencies for DI water, insulin and whole blood are 500 Hz, 350 Hz and 350 Hz, respectively. The resonance frequencies for insulin and blood are much lower than that for DI water. This results from the higher viscosity and density of the insulin and blood. According to Fig. 40, it can be seen that the resonance frequency of the pump is strongly dependent on the fluid properties.

## C. The chamber height and frequency shift

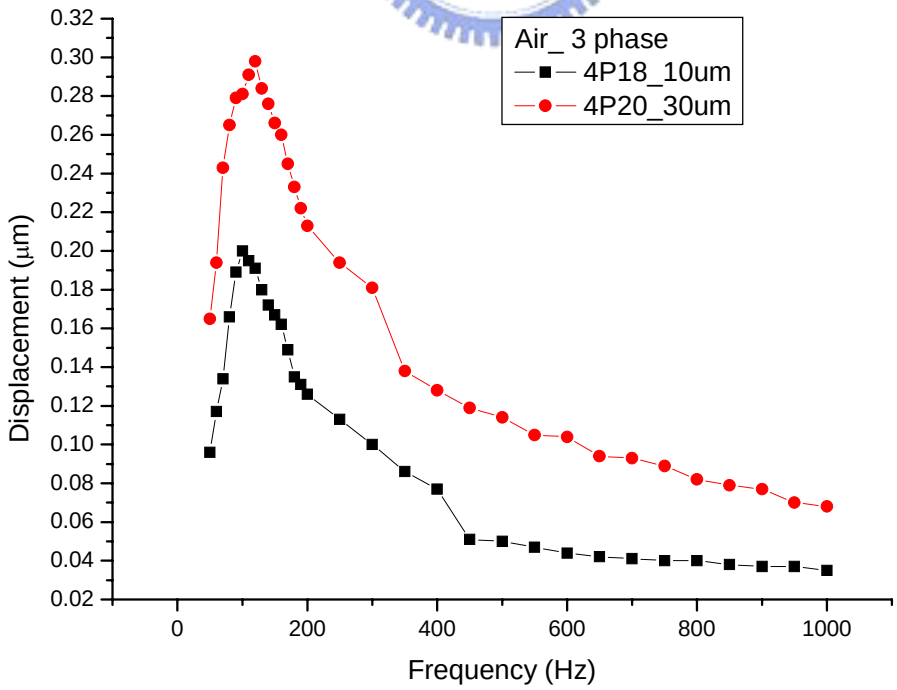


Fig. 41 The 3-phase sequence displacement frequency

response versus the chamber height.

The pump can be design for gas pumping. For higher expansion/compression ratio, we design the chamber height 10μm

$$c = \frac{\alpha \cdot 12\pi\mu a^4}{h_0^3}\left\{\left[\frac{1}{4}+\frac{1}{2}(\frac{r_0}{a})^2\right]\left[\ln(\frac{r_0}{a})-\frac{1}{2}\right]-\frac{1}{8a^4}(a^2-r_0^2)^2\right\}$$

Therefore, the damping constant $c$ is proportional to $\frac{1}{h_0^3}$.

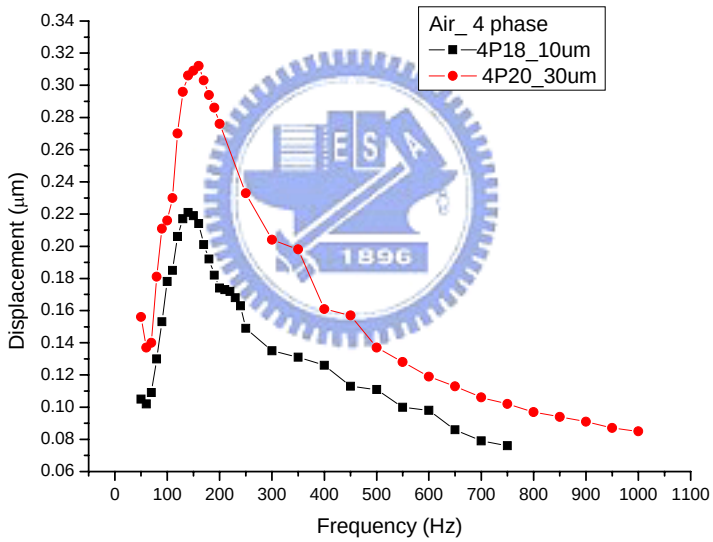


Fig. 42 The 4-phase sequence displacement frequency response versus the chamber height.

**4P18-140Hz, 4P20-160Hz**

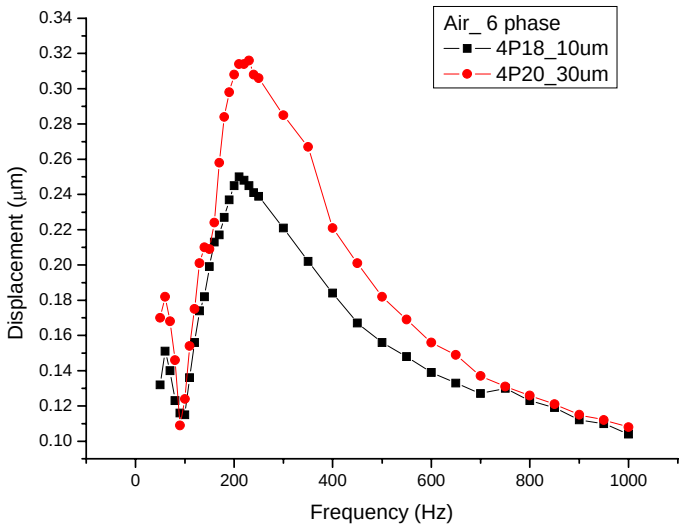


Fig. 43 The 6-phase sequence displacement frequency response versus the chamber height.

**4P18-220Hz, 4P20-230Hz**

1. The driving single connected to three chambers

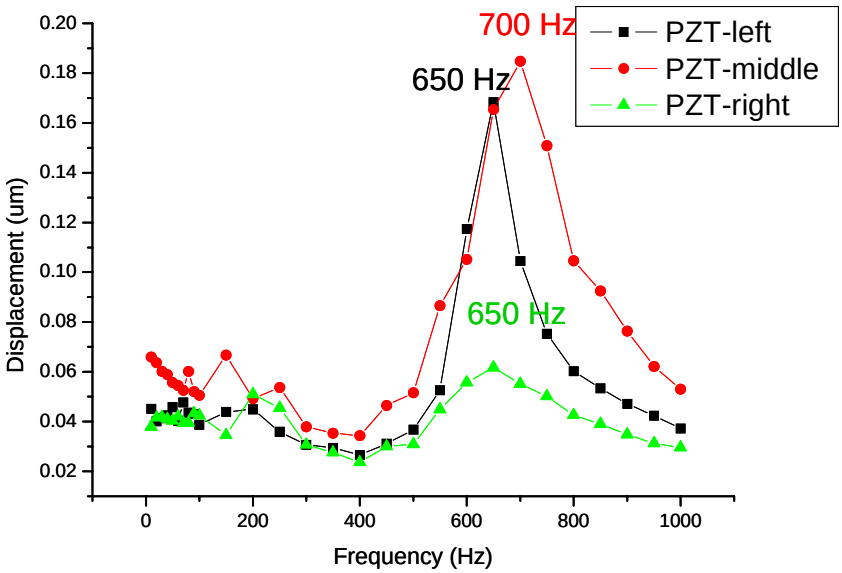


Fig. 44 4-phase three chambers driving

2. The driving single connected to just the middle chamber

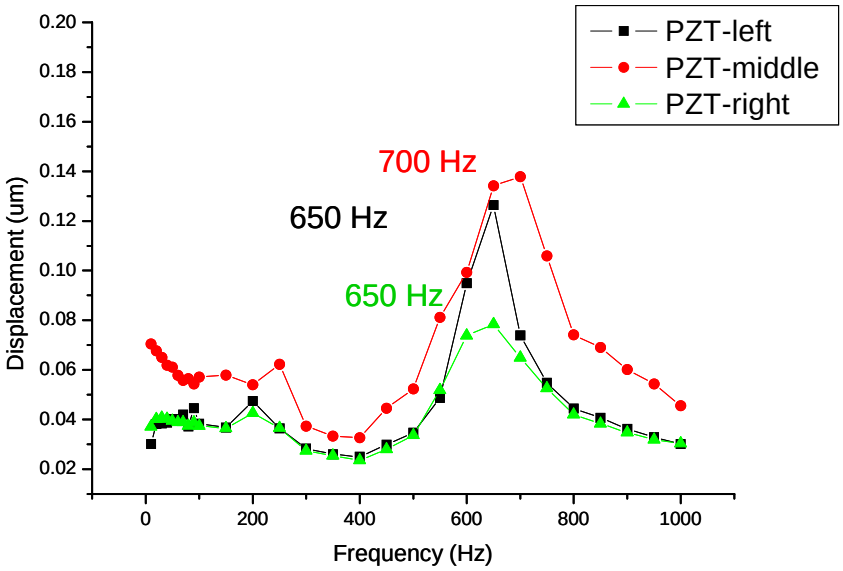


Fig. 45 4-phase the only middle chamber driving

From Fig.44 and 45, it is obvious the single connected to three chambers or just the middle chamber can affect the amplitude of the displacement frequency response without affecting their stiffness.

# The Improvement for Driving Circuit

A. Improvement of the rise time for the differential amplifier

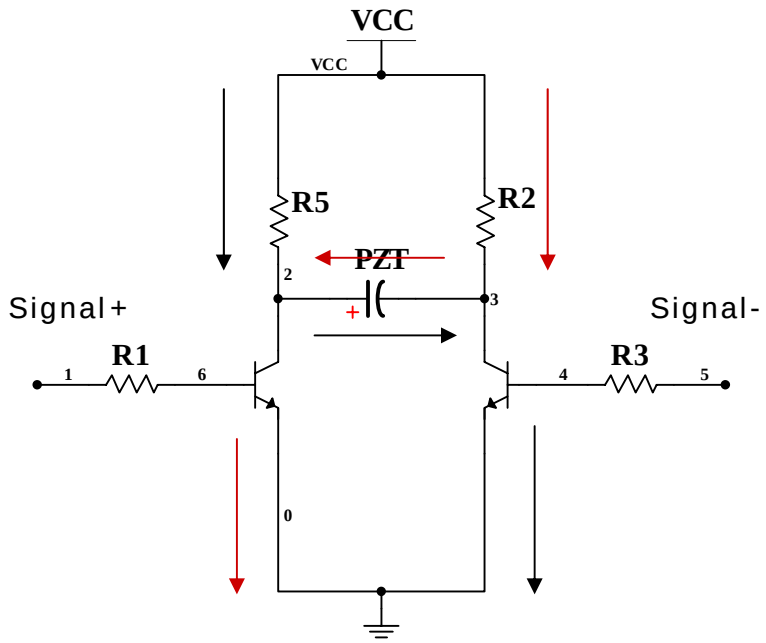


Fig. 46 The charging and discharging loop of the differential amplifier

Fig.46 indicates the charging and discharging loop of the differential amplifier. The product R C is called the "time constant", and is a characteristic quantity of the differential amplifier. The RC product can be used to determine the voltage to which any capacitor will charge through any resistance, over any period of time, towards any source voltage. The rise time will be decrease and maintain the square shape by reducing the collector resistors of the differential amplifier. The following is the testing of reducing the collector resistors in the differential amplifier to investigate the displacement (measured on the middle chamber) and flow rate.

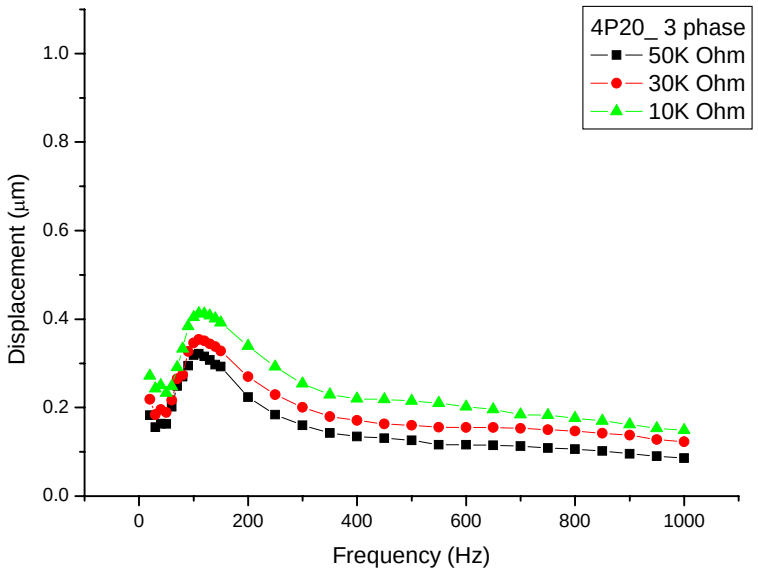


Fig. 47 The displacement vs. frequency in 3-phase sequence by reducing the collector resistance from 50 K to 10 K Ohm

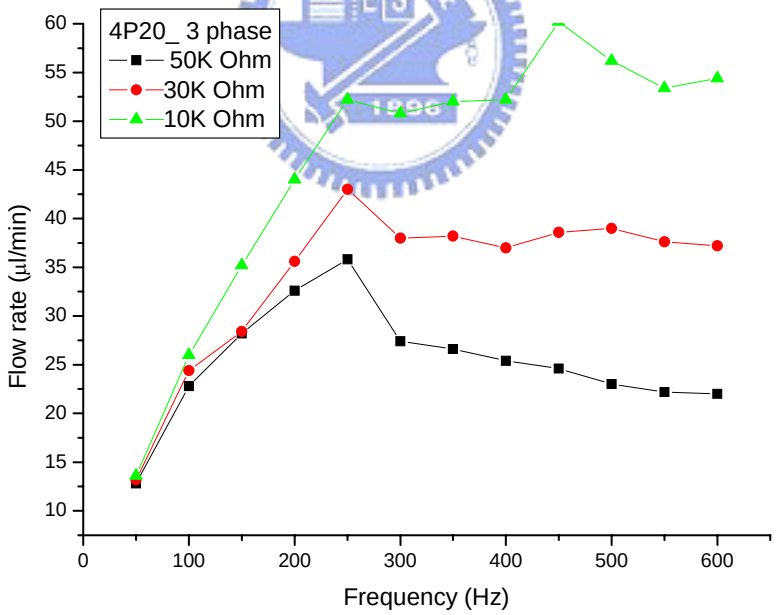


Fig. 48 The flow rate vs. frequency in 3-phase sequence by reducing the collector resistance from 50 K to 10 K Ohm

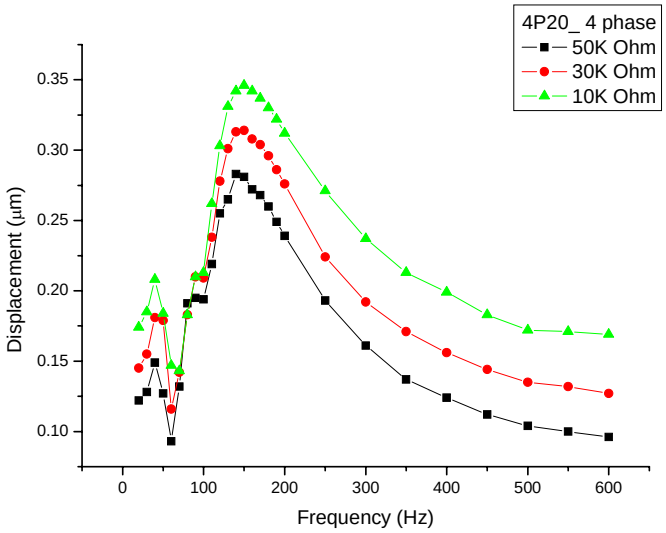


Fig. 49 The displacement vs. frequency in 4-phase sequence by reducing the collector resistance from 50 K to 10 K Ohm

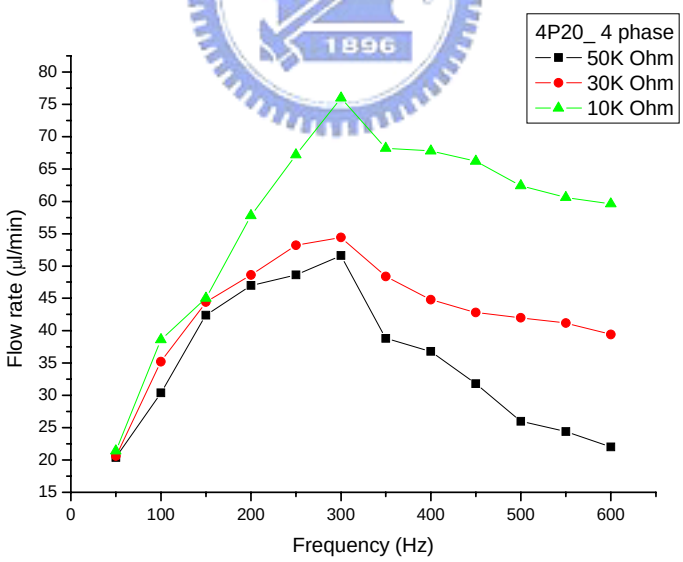


Fig. 50 The flow rate vs. frequency in 4-phase sequence by reducing the collector resistance from 50 K to 10 K Ohm

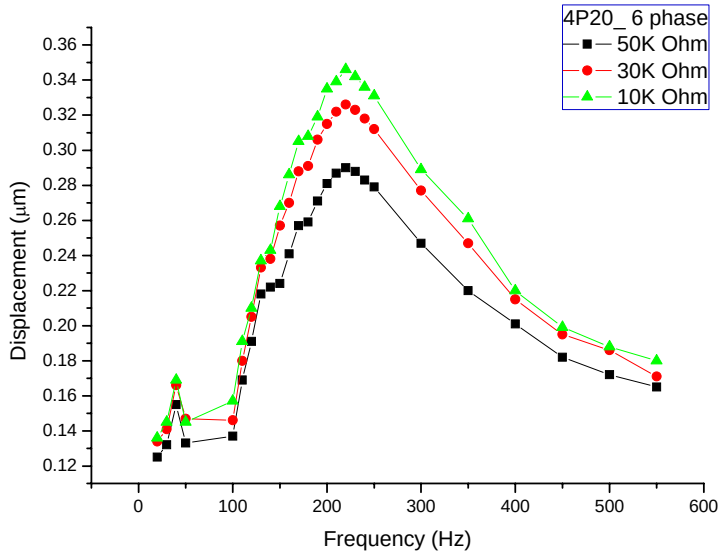


Fig. 51 The displacement vs. frequency in 6-phase sequence by reducing the collector resistance from 50 K to 10 K Ohm

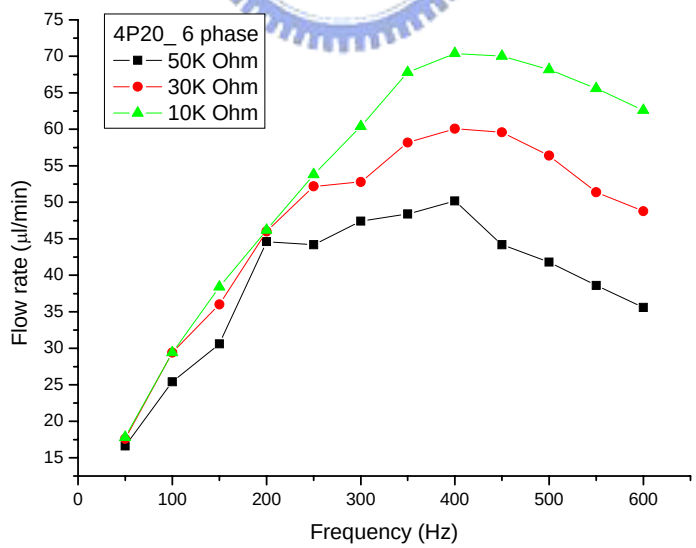


Fig. 52 The flow rate vs. frequency in 6-phase sequence by reducing the collector resistance from 50 K to 10 K Ohm

From the above observation, we know reducing the resistance at the collectors will make the displacement of the diaphragm and flow rate to increase, in 3, 4, and 6-phase sequence,

## B. Pump performance with offset driving voltage

We determined three differential situations which were the offsetting voltage upward from +80 V to -20 V, the offsetting voltage downward from +20 V to -80 V, and the voltage from +50 V to -50 V in transporting two fluids, air and DI water.

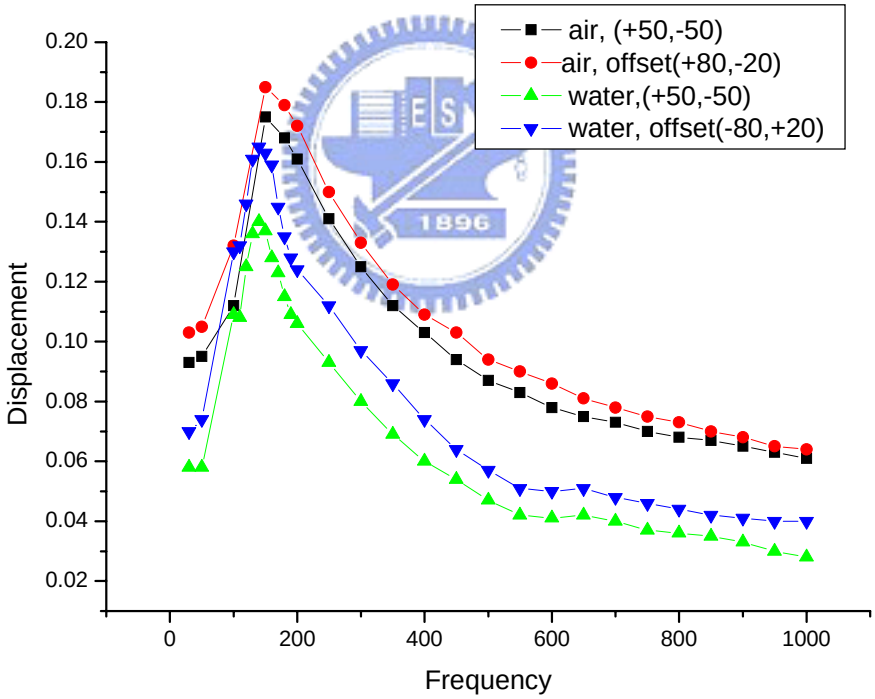


Fig. 53 The displacement vs. frequency operated in +80 V to -20 V, +50 V to -50 V and +20 V to -80 V deferential outputs

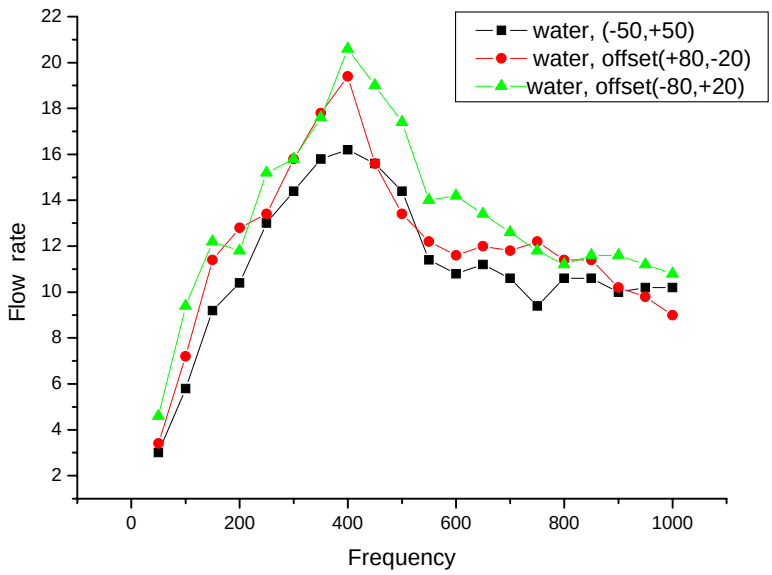


Fig. 54 The flow rate vs. frequency operated in +80 V to -20 V, +50 V to -50 V and +20 V to -80 V deferential outputs

# CHAPTER 4
# RESULTS AND DISCUSSION

## 4.1 Discussion and conclusion

During this work the simple analytical results for frequency shift based on the damping effects on the micro-diaphragm have been presented to go through the output performance on frequency domain. The so-called “simple” means we use harmonic excitation in stead of the real input signals (block wave actuation), because sinusoidal waveforms provides a basis for determining the response to a broad class of periodic inputs. The results show that not only does the added mass and added damping depend on both the fluid density and viscosity, the chamber height and actuated signals are as well for peristaltic micropumps. With fluid as the pump medium, the dynamical behaviors of the PZT actuator and the micro-diaphragm are different from those in vacuum. The damping effects on pump performance were investigated by means of the measurement of the displacement on the diaphragm at the driving voltage of 100 V and frequency varied from 50 Hz to 1 KHz. The work has proved that the principle is useful for determining the resonance frequency peak. Furthermore, the flow rate frequency response has the comparable results. Hence, to determine the resonance frequency will play a significant part in the design of the micropump performance. Besides, the driving circuit can be closely

linked with the fluid transport. The maximum flow rates of the 3-, 4- and 6-phase sequences were 21.4 μl/min, 34.6 μl/min and 36.8 μl/min at 400 Hz, 500 Hz and 700 Hz, respectively. In 3, 4, and 6-phase sequence, reducing the collector resistance will make the displacement of the diaphragm and the flow rate of the micropump to increase. The improved flow rates of the 3-, 4- and 6-phase sequences were 60μl/min, 77.5μl/min and 70μl/min at 400Hz, 500Hz and 700Hz, respectively. Therefore, the improvement design for driving circuit can enhance pump flow rate performance up to 1.9~2.8 times.

## 4.2 Outlook

The peristaltic micropump is a device with simple geometry, but very complicated dynamic fluid behavior which is very difficult to model. This work shows some of the possibilities to know a qualitative analysis of the frequency shift phenomena. Therefore, we shall concentrate further attention on the parameters determination of the $m$, $c$ and $k$ in terms of the geometric constants, working fluid properties and driving sequence to compare the performance of our pump to other peristaltic micropumps.

In addition, theoretically, peristaltic pumps need three or more pump chambers with actuating diaphragm. Most of the realized pumps have three chambers. Is there any novel idea for better design? The driving circuit design is important for pump performance. Further work is needed to optimize the driving signals and deign

better phase sequence for less leakage. The dynamic measurements and observations of the systems characteristics unfortunately seem to be difficult. Hence, the useful means of system analysis are crucially important. The CFD-ACE program may help to make sense of the system dynamics. We can load the actuated signals to simulate the squeeze motion for the increasing demand of better pump performance.

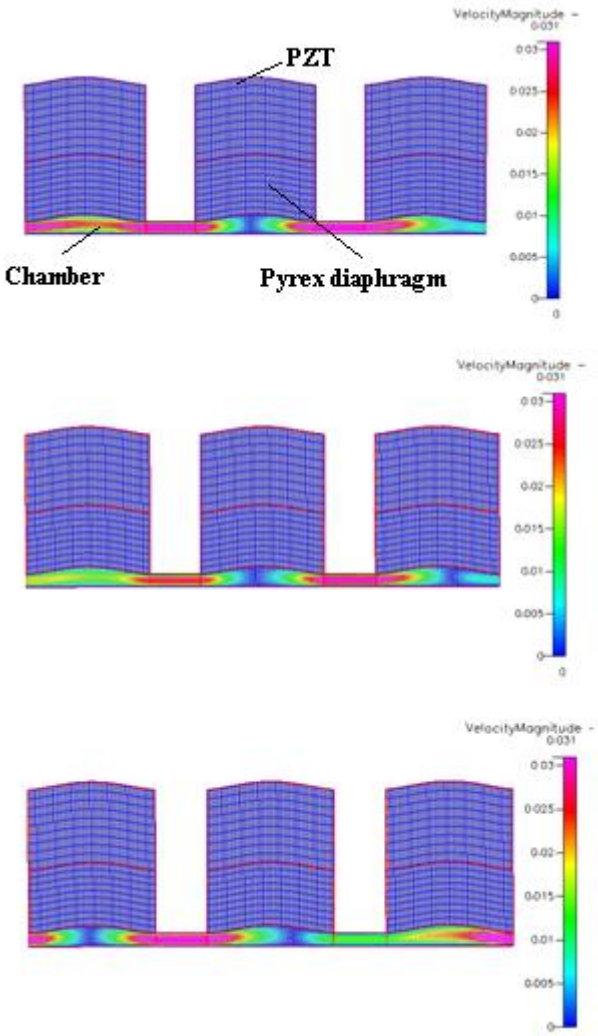


Results of the velocity field in a simplified model for the peristaltic pump (water, sine wave phase lag 0, 270, 180). The y-axis is scaled up 50 times.

# References

[1] Richard P. Feynman, There is plenty of room at the bottom, Journal of Microelectromechanical System vol. 1. No.1. March 1992

[2] A. Manz, N. Graber, H.M. Widmer, Miniaturized total chemical analysis systems: a novel concept for chemical sensing, Sens. Actuators B 1 (1990) 244–248.

[3] http://www.coventor.com/microfluidics/labonchip.html

[4] Minqiang Bu, Tracy Melvin, Graham Ensell, James S Wilkinson and Alan G R Evans, Design and theoretical evaluation of a novel microfluidic device to be used for PCR, J. Micromech. Microeng. 13 (2003) S125–S130

[5] Jing Cheng and Larry J. Kricka, Biochip Technology, Harwood Academic Publishers, 2001

[6] Johnson P. and Lloyd-Jones J.G., Drug delivery system: fundamentals and techniques, Weinheim, New York, 1987

[7] J.G. Smits, Piezoelectric micropump with three valves working peristaltically, Sensors and Actuators A21–A23 (1990) 203–206.

[8] Dae-Sik Lee, Hyun C. Yoon, Jong Soo Ko, Fabrication and characterization of a bidirectional valveless peristaltic micropump and its application to a flow-type immunoanalysis, Sensors and Actuators B 103 (2004) 409–415

[9] Woias P 2001 Micropumps—summarizing the first two decades Proc. SPIE 4560 35–52

[10] Laser D J and Santiago J G 2004 A review of micropumps J. Micromech. Microeng. 14 R35–64

[11] Peter Woias, Micropumps—past, progress and future prospects, Sensors and Actuators B 105 (2005) 28–38

[12] Nguyen,Nam-Trung and Steven T., Fundamentals and applications of microfluidics, Wereley,2002.

[13] Ahn, Chong H.; Allen, Mark G.，Fluid micropumps based on rotary magnetic actuators，Source: Proceedings of the IEEE Micro Electro Mechanical Systems (MEMS), 1995, p408-412

[14] R. Linnemann, P. Woias, C.-D. Senfft, et al., A self-priming and bubble-tolerant piezoelectric silicon micropump for liquid and gases, in: Proceedings of the 11th IEEE MEMS 1998 TechnicalDigest, Heidelberg, Germany, January 25–29, 1998, pp. 532–537.

[15] Olsson, A.; Stemme, G.; Stemme, E., Simulation studies of diffuser and nozzle elements for valve-less micropumps , Solid State Sensors and Actuators,1997. TRANSDUCERS '97 Chicago, 1997 International Conference on, Volume: 2, 16-19 June

[16] Ron L. Bardell and *et al*, "Designing high performance micro-pumps based on no-moving-parts valves," in Microelectromechanical Systems (MEMS). ASME IMECE, 1997, vol. DSC-Vol.62/HTD-Vol.354, pp. 47–53.

[17] H. Van Lintel, F. van de Pol, S. Bouwstra, A Piezoelectric micropump based on micromachining of silicon, Sensors and Actuators A15 (1988) pp.153-168

[18] Olsson A, Stemme G and Stemme E 1999 A numerical design study of the valveless diffuser pump using a lumped-mass model J. Micromech. Microeng. **9** 34–44

[19] Olsson A, Enoksson P, Stemme G and Stemme E 1997 Micromachined flat-walled valve diffuser pumps IEEE/ASME J. Microelectromech. Syst.

**6** 161–6

[20] Ullmann A, The piezoelectric valve-less pump-performance enhancement analysis, Sensors and Actuators A **69** 97–105

[21] Pan L S, Ng T Y, Liu G R, Lam K Y and Jiang T Y 2001 Analytical solutions for the dynamic analysis of a valveless micropump—a fluid–membrane coupling study Sensors and Actuators A **93** 173–81

[22] Pan L S, Ng T Y, Wu X. H and Lee H P, Analysis of valveless micropumps with inertial effects, J. Micromech. Microeng. **13** (2003) 390–399

[23] Tikeswar Naik, Ellen K. Longmire, Susan C. Mantell, Dynamic response of a cantilever in liquid near a solid, Sens. Actuators A 102 (2003) 240–254.

[24] Kan Junwu, Yang Zhigang, Peng Taijiang, Cheng Guangming, Wu Boda, Design and test of a high-performance piezoelectric micropump for drug delivery, Sensors and Actuators A 121 (2005) 156–161

[25] B Husband, M Bu, A G R Evans and T Melvin, Investigation for the operation of an integrated peristaltic micropump, J. Micromech. Microeng. 14 (2004) S64–S69

[26] Nam-Trung Nguyen, Xiaoyang Huang, Miniature valveless pumps based on printed circuit board technique, Sensors and Actuators A 88 (2001) 104-111

[27] T. Ikeda ,Fundamentals of Piezoelectricity, Oxford ;Oxford University Press,1990.New York

[28] Xing Yang et al. , A micro diaphragm air pump for air supply of micro fuel cell, proceedings of transducers'05, 13th international conference on solid-state sensors, Actuators and Microsystems, Seoul,Korea,2005

[29] Fox and McDonald, Introduction to fluid mechanics, New York: Wiley,

1990.

[30] Timoshenko S. P. and Weaver, W., Vibration Problems in Engineering, 4th ed., John Wiley, New York, 1974.

[31] http://www.piezo.com/prodsheet2sq5H.html#priceinfo